ABSTRACT

STRUCTURAL MECHANISMS OF (POLY)ANION SOLID SOLUTION IN SYNTHETIC OH-Cl BINARY APATITE AND NATURAL F-OH-Cl TERNARY APATITE

by Sean Robert Kelly

This thesis comprises two separate manuscripts prepared for submission to the American Mineralogist: “Solid solution in the apatite OH-Cl binary system: compositional dependence of solid solution mechanisms in calcium phosphate apatites along the Cl-OH binary” and “Column anion arrangements in chemically zoned ternary chlorapatite and fluorapatite from Kurokura, Japan”. The research characterizes the detailed structural mechanisms that enable solid solution among fluorine (F), hydroxyl (OH), and chlorine (Cl) in the mineral apatite using single-crystal x-ray diffraction and electron microprobe analysis. The first manuscript, using synthetic apatite samples, documents three previously unseen structural modifications (column anion arrangements) of apatite that enable the binary solid solution between OH and Cl. The second manuscript serves to compliment the first by demonstrating one of these structural mechanisms in a natural ternary apatite, while simultaneously documenting a fourth new apatite structural modification that occurs in F and OH rich, and Cl poor apatite.

STRUCTURAL MECHANISMS OF (POLY)ANION SOLID SOLUTION IN SYNTHETIC OH-Cl BINARY APATITE AND NATURAL F-OH-Cl TERNARY APATITE

A Thesis

Submitted to the

Faculty of Miami University

in partial fulfillment of

the requirements for the degree of

Master of Science

by

Sean Robert Kelly

Miami University

Oxford, Ohio

2016

Advisor: John Rakovan

Reader: Dan Harlov

Reader: Mark Krekeler

This Thesis titled

STRUCTURAL MECHANISMS OF (POLY)ANION SOLID SOLUTION IN SYNTHETIC OH-Cl BINARY APATITE AND NATURAL F-OH-Cl TERNARY APATITE

by

Sean Robert Kelly

has been approved for publication by

The College of Arts and Science

and

Department of Geology

_____

John Rakovan

_____

Daniel E. Harlov

_____

Mark Krekeler

Table of Contents

List of Tables

Chapter 1:

Chapter 2:

List of Figures

Chapter 1:

Chapter 2:

Dedication

I dedicate this work to my loving and supportive family: Ian Kelly, Evan Kelly, Sharon Kelly, Clay Kelly, Vanera Livingston, Bob Livingston, Roseanne Kelly (for her love of rocks) and Ed Kelly.

Acknowledgements

I acknowledge the entire geology department at Miami (in particular John Rakovan, Mark Krekeler, and the geology graduate student body) for their tremendous support during my time at Miami University. I also acknowledge John Hughes for sharing his crystallography expertise with me. I could not have achieved this work without them.

Solid solution in the apatite OH-Cl binary system: compositional dependence of solid solution mechanisms in calcium phosphate apatites along the Cl-OH binary

Published in American Mineralogist Volume 101, pages 1783-1791, 2016

JOHN M. HUGHES[1]
[1]Department of Geology, University of Vermont, Burlington, Vermont 05405, U.S.A.

DANIEL HARLOV[2,3]
[2]GeoForschungsZentrum Potsdam, Telegrafenberg, D-14473 Potsdam, Germany

[3]Department of Geology, University of Johannesburg P.O. Box 524, Auckland Park, 2006 South Africa

SEAN R. KELLY[4], **JOHN RAKOVAN**[4]
[4]Department of Geology and Environmental Earth Science, Miami University, Oxford, Ohio 45056, U.S.A.

MAX WILKE[2]
[2]GeoForschungsZentrum Potsdam, Telegrafenberg, D-14473 Potsdam, Germany

ABSTRACT

The method of accommodation of solid solution along the OH-Cl binary in calcium phosphate apatites is not fully understood; because of steric constraints in mixtures of OH and Cl anions in the apatite [0,0,*z*] anion column, the positions of OH and Cl anions in the pure hydroxylapatite and chlorapatite endmembers cannot coexist in the binary anion column. We have undertaken high-precision single-crystal X-ray structure studies of eight synthetic samples along the OH-Cl apatite binary ($R_1 \leq 0.0159$). We found that for all samples solid solution is attainable in space group $P6_3/m$, but the particular method of solid solution is dependent on composition. For samples with Cl > OH, three column anion sites (two for Cl, one for OH) provide allowable bond distances with the Ca2 atoms and allow a sequence of column anions that provides sufficient anion-anion distances and also effects reversal of the sense of ordering of the column anions relative to the mirror planes at z = ¼ and ¾. In a sample with OH > Cl, three sites exist in the anion column that also provide allowable bond distances to the triangle of Ca2 atoms or its disordered Ca2' equivalent, and afford a sequence of atoms that permits reversal of the anion column and maintenance of $P6_3/m$ symmetry. One of those sites is occupied by OH, and provides acceptable Ca2-OH distances, and another accommodates Cl with ideal Ca2-Cl distances. A third column anion site is unique among the calcium phosphate apatites. That site, termed the ClOH site, accommodates *both* OH and Cl. The site has an ideal bond distance for OH to the Ca2 atoms in the Ca2 triangle, and also has an ideal bond distance for a Cl occupant to disordered Ca2' atoms; thus, because of the disordering of the Ca2-Ca2' atoms, a single site can accommodate either anion with ideal, but disparate, bond distances to Ca. Finally, in OH-Cl

apatites with OH ≈ Cl, also crystallizing in space group $P6_3/m$, four anion positions are occupied in the anion column, including the ClOH site that allows occupancy by both OH and Cl. In addition to that site and distinct OH and Cl sites, OH is found to occupy the site within the mirror plane at (0,0,1/4), the site occupied by F in F-bearing apatite. Occupancy of that site is essential to reversing the sense of ordering of the anion column relative to the mirror planes and preserving $P6_3/m$ symmetry. Thus, the methods of effecting solid solution along the OH-Cl are composition-dependent and complex.

Keywords: apatite, hydroxylapatite, chlorapatite, solid solution, binary, crystal structure

INTRODUCTION

Apatite is the most abundant phosphate mineral on Earth and a phase with fundamental importance in geology, agriculture, materials science, medicine and dentistry. In addition to the apatite that forms in igneous, metamorphic, sedimentary, and hydrothermal environments, all hard tissue of the human body except small parts of the inner ear is formed of apatite materials, indicating a remarkable link between the inorganic and organic genesis for the mineral; apatite is among the few most common biominerals on Earth. In addition, apatite forms the foundation of the global phosphorus cycle. The importance of apatite in many disciplines, indeed in even sustaining human life as the chief source of phosphate for fertilizer, cannot be overstated. The reader is referred to a recent *Elements* issue (V. 11, June, 2015) that is devoted entirely to apatite for a more detailed account of the chemistry, structure, and applications of the mineral.

Apatite *sensu lato* has a composition of $Ca_{10}(PO_4)_6(OH,F,Cl)_2$, and is one of the more rare *anion* solid solutions among minerals. Despite the importance and ubiquitous nature of the mineral, details of the apatite atomic arrangement have not been forthcoming. Hughes et al. (1989) demonstrated that the positions of the [0,0,*z*] column anions in the apatite end-members (fluorapatite, chlorapatite, and hydroxylapatite) are not compatible in solid solution because of steric constraints. This has led to speculation on how solid solution is effected in apatite *sensu lato*, but definitive structures on all the binaries are not extant. Hughes (2015) summarized the apatite atomic arrangement and the state of our knowledge of the apatite structure, and illustrated the conundrum of the steric constraints among the anions. We refer the reader to that work for a summary of the apatite atomic arrangement.

For any combination of anion occupants, the positions of the anions in the [0,0,*z*] anion column result from several factors, including the size of the particular column anions, the nearest-neighbors in the anion column and electrostatic repulsions therefrom, any dissymmetrization that is present in the structure, electrostatic attractions to the surrounding triangle of Ca2 atoms, and, in hydroxylapatite, the hydrogen bonding that occurs from the hydroxyl hydrogen to neighboring column anions. Hughes et al. (1990) demonstrated that in ternary apatite, solid solution among all three column anions was achieved in two different ways. They examined a low-temperature, metamorphic apatite that accommodated all three column anions by reducing the typical hexagonal $P6_3/m$ apatite symmetry to monoclinic $P2_1/b$ symmetry, a dissymmetrization resulting from ordering of the anions. In a high-temperature volcanic apatite, they demonstrated that accommodation of all three column anions is made possible by occupation of a second Cl site, one not seen in the pure chlorapatite end-member, a site that shifts the Cl atom closer to its associated mirror plane and provides sufficient distance for a neighboring hydroxyl. A sequence of anions can thus be erected that allows sufficient distance between all nearest-neighbors in the anion column and also allows reversal of the sense

of local order relative to the mirror planes at [0,0,1/4] and [0,0,3/4] (column reversal), thus effecting the $P6_3/m$ symmetry over the crystal as a whole.

Although the accommodation of three anions in the apatite anion column has been illustrated, the anion positions along the three binary joins in the F-OH-Cl apatite ternary are more problematic (McCubbin et al. 2008). Hughes et al. (2014a) showed that in synthetic $P6_3/m$ F-Cl apatite, the two disparate ions are accommodated by the creation of an off-mirror fluorine site that allows sufficient anion-anion distances and also allows column reversal; Hughes et al. (2014b) also showed that a natural F-Cl analog with the same anion accommodation method occurs in the Three Peaks area of Utah.

Young et al. (1969) investigated the accommodation of anions in F-OH binary apatite using nuclear magnetic resonance spectroscopy. They noted that in the anion column the fluorine atom shifts at least 0.1Å off the mirror plane when in an environment of asymmetric hydrogen bonding. Their study demonstrated that asymmetric hydrogen bonding (OH-F) or symmetric hydrogen bonding (OH-F-HO) "secures" the F more strongly in the anion column, and this enhanced bond strength inhibits hydroxyl diffusion along the anion column. They invoked this fact to explain the observation that solubility of hydroxylapatite decreases with substituent fluorine in the anion column, as diffusion of hydroxyl is a component of dissolution of apatite; such an observation is particularly germane in the fluoridation of tooth enamel as a prophylaxis for dental caries.

The accommodation of OH and Cl in the binary apatite anion column is less well understood. The positions of the anions in the endmembers do not provide an atomic arrangement that yields sufficient distances between the anions nor does it provide a mechanism for column anion reversal. Garcia-Tunon et al. (2012) also undertook a study on synthetic apatite, and described a model for accommodation of the two anions in the binary anion column. However, the use of anisotropic thermal parameters for the column anions, as employed in that study, creates difficulties in refinement by obscuring sites with small occupancy by large values of U_{33} of other column anions (Hughes et al. 2014a), and thus the present study was undertaken.

To determine the structural compatibility of any two anions in the apatite anion column, we have synthesized crystals along the three binaries in the (F-OH-Cl) apatite ternary system and undertaken single-crystal X-ray structure studies on those crystals. Here we report the atomic arrangements of members of the OH-Cl binary, and illustrate the several ways that solid solution can be effected. The compositions of the studied crystals along the OH – Cl binary are illustrated in Figure 1.

SOLID SOLUTION APATITE BINARIES: THE CONUNDRUM

The radii of the three occupants of the apatite anion columns (F = 1.30Å, Shannon and Prewitt 1969; Cl = 1.72Å, OH = 1.33Å; Jenkins and Thakur 1979) differ greatly, with Cl being much larger than F and OH. In addition the three anions exist in [0,0,z] columns at the edges of the unit cells, and those columns are intersected by {0,0,ℓ} mirror planes at z = ¼ and ¾ (Figure 2). Most commonly, the apatite compounds are hexagonal, crystallizing in space group $P6_3/m$, but trigonal and monoclinic subsymmetries do exist in more rare apatite compounds (Hughes and Rakovan 2015).

Where F occupies the anion column, it occurs in a site that is contained within the mirror plane, at (0,0,¼) or (0,0,¾); that site is surrounded by a triangle of Ca2 atoms. For OH- or Cl-bearing apatites, however, the OH and Cl column anions are too large to fit in the center of the triangle of Ca2 atoms. Thus, the hydroxyls are displaced ~0.35Å above *or* below its associated

mirror plane, and the larger Cl atoms are displaced ~1.3Å above *or* below its associated mirror plane. Therefore, with an F atom site, true mirror symmetry is maintained in each unit cell; at OH- and Cl-occupied sites, although local mirror symmetry is not present at any mirror plane, average mirror symmetry is attained over the crystal as a whole, as the OH and Cl sites above and below the mirror plane are all half-occupied. This is only strictly true when OH or Cl are disordered, above and below the mirror, over the entire structure.

In apatites that contain mixtures of the column anions, if indeed they crystallize in space group $P6_3/m$, the sequence of column anions must allow for reversals of the sense of ordering in the anion column, i.e., allow for reversal of anions from ordered above the plane to below the plane, and the converse, and also provide sufficient anion-anion distances for coexistence of column anions. Figure 3 illustrates the conundrum by showing the maximum anion-anion distances in the anion column that can be achieved using the anion positions in the hydroxylapatite and chlorapatite hexagonal endmembers (Hughes et al. 1989). Clearly, the endmember OH and Cl anion positions are not compatible in the OH-Cl binary column, yielding a Cl-O(H) distance of 2.53Å and an H-H distance of 0.83Å.

Below we describe the synthesis of samples along the OH-Cl binary, provide the details of the crystal structure studies of their atomic arrangements, and illustrate how the criteria for $P6_3/m$ symmetry are met for three different ranges of composition along the OH-Cl calcium apatite binary.

Synthesis of apatite samples

Apatites across the Cl-OH join were synthesized utilizing Cl-OH exchange between synthetic pure end member chlorapatite and a series of $Ca(OH)_2$-H_2O solutions at 1100 °C and 400 MPa. Synthesis of a large size range of chlorapatite crystals up to 5 or more mm in length was achieved by dry mixing 0.03 moles (9.3 grams) of $Ca_3(PO_4)_2$ into 0.1 moles of $CaCl_2$ (11 grams). This mix was taken up to 1375 °C in a covered Pt crucible in open air, soaked at 1375 °C for 15 hours, and then slowly cooled to 1220 °C at 3 °C per hour after which the crucible was removed from the oven and air cooled (see Schettler et al. 2011). The chlorapatite crystals were released from the flux by boiling the crystal/flux mass in 2 liters of distilled H_2O followed by several additional washings.

Apatites across the Cl-OH join were then synthesized by exchanging 400 mg of a 200 – 500 μm size separate of these synthetic chlorapatites with 25 – 200 mg of a $Ca(OH)_2$-H_2O solution with variable proportions of $Ca(OH)_2$ and H_2O. Each of the chlorapatite-$Ca(OH)_2$-H_2O mixes were sealed in a 4 cm long, 5 mm diameter Pt capsule and taken up to 1100 °C and 400 MPa in an internally heated gas pressure vessel using Ar as the pressure medium. Run duration was 3 – 6 days. The temperature was measured with 3 S-type thermocouples and calibrated based on measurements of the melting points of NaCl at 843 °C/200MPa and 904 °C/500 MPa (Akella et al. 1969). The accuracy is about ±5 °C at 200 MPa and ± 20 °C at 500 MPa. Maximum thermal gradients along the capsules were ±10 °C. Pressure measurement was done with a strain gauge and was accurate to ±7 MPa for experiments up to 500 MPa. During the experiment, pressure was controlled automatically within ±5 MPa using the hydraulic system of the intensifier and a programmable control unit. The samples were heated isobarically with a rate of 30 °C/min and quenched isobarically with quench rates of 150–200 °C/min.

During the experiment the following total exchange took place between the chlorapatite crystals and the $Ca(OH)_2$-H_2O solution via a coupled dissolution-reprecipitation process (see Putnis 2009):

$$Ca_5(PO_4)_3Cl + Ca(OH)_2 = Ca_5(PO_4)_3(Cl,OH) + CaCl_2 \quad (1)$$

and

$$Ca_5(PO_4)_3Cl + H_2O = Ca_5(PO4)_3(Cl,OH) + HCl \quad (2)$$

After quench the Pt capsule was opened and the exchanged Cl-OH apatites removed and washed 4 – 5 times in a 100 ml beaker of doubly distilled H_2O at room temperature to remove the $CaCl_2$, HCl, and whatever $Ca(OH)_2$ remained. The washed Cl-OH apatite crystals were then air dried at room temperature.

Details of X-ray structure studies

X-ray diffraction data were collected with a Bruker Apex II CCD single-crystal diffractometer using graphite-monochromated Mo K_α radiation. For each sample, redundant data were collected for a sphere of reciprocal space (4,500 frames, 0.20º scan width; average redundancy ≈ 16) and were integrated and corrected for Lorentz and polarization factors and absorption using the Bruker Apex2 package of programs. The atomic arrangement was refined in space group $P6_3/m$, on F^2, with SHELXL-97 (Sheldrick 2008) using neutral atom scattering factors and full-matrix least-squares, minimizing the function $\Sigma\, w(F_o^2 - F_c^2)^2$ with no restraints. All atoms were refined with anisotropic temperature factors except the column anions; an extinction coefficient was also refined. As noted previously, in earlier studies it was found that the use of anisotropic atomic displacement factors for the column anions yields unreasonable values of U_{33}, an anisotropy that masks the positions of anion sites occupied by small fractions of a column anion. The occupancy values of the column anions were not constrained.

After initial refinements of the structure, the column anion positions were located using difference maps. In addition to those peaks, in many of the structures the largest peak in the difference map was located near the Ca2 atom, suggesting that the peak resulted from disorder of Ca2 in response to the different local bonding environments provided by the adjacent column anions, a common occurrence in apatites with mixed occupants in the anion column (Hughes *et al*. 1990). That disorder was successfully modeled in the structures where the Ca2' peak was noted (i.e., all structures with OH ≈ Cl and OH > Cl).

As will be described subsequently, there is a partially occupied site in the anion column that can contain either Cl or OH because of disorder of the surrounding Ca2 atoms, termed the ClOH site. To model occupancy of that site, the site occupancy was first refined with Cl scattering factors. Because we were thus modeling a site with mixed O(H) and Cl occupancy, modeling that site with Cl atoms invariably yielded a total anion column occupancy less than the necessary 2.00 *apfu*, and modeling the electron occupancy with O(H) invariably led to a total anion occupancy greater than 2.00. We then determined how many atoms were needed to fill the anion column to 2.00 *apfu*, and apportioned the electron occupancy of that site to a combination of O(H) and Cl that maintained the total electron occupancy and filled the anion column to 2.00 *apfu*. The validity of the assumption of a full anion column is demonstrated by the refinement of three of the samples *without* a ClOH site, which yielded total anion column occupancy of 2.02, 2.04, and 2.01 anions in unconstrained refinements.

RESULTS OF THE STRUCTURE STUDIES

The results of the structure studies of the crystals along the OH-Cl apatite binary suggest the accommodation of OH and Cl can occur in three ways, depending on the composition of the binary apatite. Below we summarize those accommodations and illustrate the column anion

arrangement in apatites along the OH-Cl binary. First, however, a few comments on disorder in the apatite structure are appropriate.

The anion columns in apatite are surrounded by a triangle of Ca2 atoms (Fig. 2). As the column anions vary within the apatite anion column, it has been shown (Sudarsanan and Young, 1978; Hughes et al., 1990) that the Ca2 atoms in the triangle can disorder into a second position, herein called Ca2', to respond to the particular nearest-neighbor column anion, with Ca2-Ca2' distances on the order of 0.3Å. In the structures in this paper in which the Ca2' position was among the three largest difference peaks in the penultimate Fourier electron density difference map, we modeled the Ca2' site in the structure. That disorder also propagates to oxygen atoms, particularly O3. However, disorder of oxygen atoms that propagates from disorder of the Ca2 atoms is difficult to model in part due to their relatively small scattering factors, and thus oxygen disorder was not modeled in this study. The disorder of the Ca2 atoms is particularly important in creating a unique anion column site, as will be explained subsequently.

BINARY APATITES WITH Cl > OH.

We examined three samples of OH - Cl apatite that have Cl > OH (Figure 1). The contents of the anion columns in these crystals, as determined by the single-crystal structure refinements, are $[Cl_{1.65}(OH)_{0.37}]$ (sample APS78), $[Cl_{1.66}(OH)_{0.38}]$ (sample APS82), and $[Cl_{1.75}(OH)_{0.26}]$ (sample APS83). The samples provided superior refinements, with R_1 values of 0.0157, 0.0148, and 0.0158, respectively. In those samples, we found the symmetry is indeed hexagonal, $P6_3/m$; reversal of the anion column to achieve this hexagonal symmetry occurs with a single O(H) site and two Cl sites. We have deposited the complete details of the data collection, structure refinement and results of the structure studies for these samples APS78, APS82, and APS83. For the reader's convenience, Table 1 contains the atomic coordinates and equivalent atomic displacement parameter for one of the samples, APS83, and the interatomic distances we note below are from that sample.

The anion column reversal sequence for apatites along the OH-Cl binary with compositions with Cl > OH is depicted in Figure 4, and the *z* coordinates of the column anion sites and their percentage of the total occupancy are given in Table 2. As seen in Table 2, three positions exist in the anion column, two of which accommodate Cl atoms and one that accommodates OH occupants. In the apatites with Cl > OH, the OH anion is located at a single site at $z \approx 0.183$, slightly farther from the mirror plane than in endmember hydroxylapatite; that OH bonds to three Ca2 atoms at 2.525Å distance. Cl is accommodated in a site at $z \approx 0.06$ (labeled Cl_a), similar to the location in hexagonal chlorapatite, and bonds to three Ca2 atoms at distances of 2.812Å. A second Cl site (Cl_b) at $z \approx 0.105$ also presents a bonding environment that accommodates Cl, at a distance of 2.677Å from each of three Ca2 atoms. In the three samples analyzed with Cl > OH, the occupancy of the two Cl sites demonstrates that approximately twice as many Cl_a sites are occupied as Cl_b sites.

The anion column depicted in Figure 4 illustrates an anion sequence that allows reversal of the anion column and acceptable anion-anion distances. The minimum 3.08Å Cl-Cl distance is at the lower end of observed Cl-Cl distances in a recent compilation (~3.0 - ~4.0Å; Vener et al. 2013), but is within the range of observed Cl-Cl contacts. The other distances that are derived from this set of anion column sites are an OH-Cl distance of 2.85Å and an OH-OH distance of 2.49Å. The latter distance is somewhat short for an O-O distance, but in the range typical for a hydrogen bonded O-H···O distance with strong hydrogen bonding. Brown (1976) distinguishes between weak hydrogen bonds (O-O > 2.7Å) and strong hydrogen bonds (O-O < 2.7Å), and

noted that the strong hydrogen bonds tend to be linear and weak hydrogen bonds tend to be bent. In the apatite anion column, the hydrogen bonds will always be linear, and thus the observed O-O distance, that we assume is hydrogen bonded, is of an ideal distance. Although in this work we have not located the H atoms in the column hydroxyls, we can thus suggest that hydrogen bonding occurs between two adjacent hydroxyls to yield the 2.49Å OH-OH distance. We comment subsequently on hydrogen bonding in the OH - Cl apatite anion column.

It is of interest to note, and germane to the other methods of column reversal along the OH - Cl apatite anion column for compositions of OH ≈ Cl and OH > Cl, that there is no disordering of the Ca2 atom detected in the structures with Cl > OH. As will be illustrated subsequently, that disorder is necessary for the other methods of accommodation of column reversal, but not for the configuration in samples with Cl > OH.

BINARY APATITES WITH OH > Cl.

We have synthesized a single sample with OH > Cl, and we found it has a method of reversing the anion sequence and preserving $P6_3/m$ hexagonal symmetry in the OH-Cl apatite anion column that has not been previously recognized. We have deposited the complete details of the data collection, structure refinement and results of the structure studies for sample APS76. For the reader's convenience, Table 3 contains the atomic coordinates and equivalent atomic displacement parameter for the sample; the sample provided a superior refinement, with R_1 = 0.0149. Note that sample APS76 contains disordered Ca2 atoms, as a portion of the Ca2 atoms are disordered into Ca2' sites approximately 0.3Å distant.

Table 4 lists the *z* coordinates of the (0,0,*z*) column anion positions as well as the portion of each site that is occupied. As seen in Table 4, a column anion site occurs at *z* = 0.154 (labeled ClOH), a column anion site not previously recognized in any apatite study and a site approximately midway between endmember Cl sites and OH sites. Accompanying that site are an OH site at z = 0.202 (2.381Å distant from Ca2), essentially at the OH site found in endmember hydroxylapatite, and a Cl_b site at *z* = 0.083 (2.623Å distant from Ca2), near the Cl site in endmember chlorapatite.

The reversal of the anion column using these sites to facilitate $P6_3/m$ symmetry is illustrated in Figure 5. Of particular interest in the OH-Cl binary anion column is the newly discovered ClOH site. As mentioned and referenced previously, the Ca2 atoms in apatites with more than one column anion can disorder to allow the Ca2 atoms to occupy positions that provide ideal bond distances to the particular column anion (F, OH, Cl) associated with the mirror plane that contains the Ca2 (Ca2') triangle. Along the OH-Cl binary, with samples that contain OH > Cl, the ClOH site occupies a unique position that accommodates *both* Cl and OH at ideal bond distances with the surrounding Ca2 triangle, one anion at an ideal bond distance with Ca2, and the other at an ideal bond distance with the disordered Ca2' atoms.

The ClOH positon at *z* = 0.154 in sample APS76, with OH > Cl, provides a bond distance between the Ca2 site and O(H) occupying the ClOH site of 2.45Å, and the disordered Ca2' atom has a bond distance of 2.72Å to a Cl atom in the ClOH site. Both bond distances are nearly ideal for the respective anions to Ca; thus, a single column anion site can accommodate both Cl and OH at ideal bond distance to the neighboring Ca2 atoms, with O(H) bonding to a Ca atom and Cl bonding to its disordered equivalent Ca2' atom. This is the first time such a site has been observed in the apatite anion column, and serves to illustrate the robust nature of accommodation of column anions in the apatite atomic arrangement.

BINARY APATITES WITH OH ≈ Cl.

We have synthesized four samples with OH ≈ Cl in the OH-Cl apatite column (Figure 1). Those samples, like those with OH > Cl and Cl > OH, present a unique method of reversing the sequence of the anion column and preserving $P6_3/m$ symmetry. We have deposited the complete details of the data collection, structure refinement and results of the structure studies for these samples APS71 (R_1 = 0.0159), APS72 (R_1 = 0.0151), APS74 (R_1 = 0.0155), and APS80 (R_1 = 0.0155). For the reader's convenience, Table 5 contains the atomic coordinates and equivalent atomic displacement parameter for one of the samples, APS71, and the interatomic distances we note below are from that sample. Table 6 lists the *z* coordinates and percentage occupancy for the four occupied sites in the anion column; that set of occupied sites is unique in the calcium phosphate apatites.

Figure 6 depicts the method of reversal of the anion column in the OH-Cl anion column with OH ≈ Cl. As illustrated there and listed in Table 6, there is a Cl site (Cl_a) at (0,0,0) in which a small portion of the sites are occupied (< 5% on average of the structures studied); this site is occupied by Cl in the F-Cl binary apatites (Hughes et al. 2014a) but was not previously noted in OH-Cl binary apatites. Because the position of that Cl atom is halfway between two mirror planes (z = -¼, z = +¼), Cl atoms in that site bond to six Ca2 atoms rather than three, leading to longer Ca2-Cl bond lengths (Ca2-Cl_a distance = 2.908Å) that are sufficient to match the bond valence sum of the Cl.

We can suggest that the Cl site at (0,0,0) is partially occupied by OH, in a mechanism suggested by Mackie and Young (1974). In their deduction of anion positions in the fluor-chlorapatite anion column, Mackie and Young suggested three criteria, paraphrased here: 1) the interatomic distances between occupants of the anion column must be of reasonable length, 2) the anions must occupy positions found in the structure refinement, and 3) F can occupy a Cl site but Cl cannot occupy an F site because of the resulting short Ca-Cl distances. It is this third criterion that demonstrates how the Cl site at (0,0,0) can exist, and we can rewrite their conclusion #3 for hydroxyl-chlorapatite by substituting "OH" for "F" in their discussion.

Figure 6 depicts an anion sequence in which one Cl*a* site (that site at z = 0, 1/2) is occupied by a hydroxyl. In that sequence, the presence of that OH allows sufficient distance between that anion and an adjacent Cl_b anion, identical to the mechanism noted for F-Cl apatite by Mackie and Young (1974) and Hughes et al. (2014a, b). Relatively few of the Cl positions are of type Cl*a* (< 5%), but, as predicted by Mackie and Young (1974), they do exist. The presence of these sites is effected by a column OH anion occupying a Cl site, yielding an acceptable OH-Cl distance in the anion column; however, all of those sites need not be occupied by OH.

In the anion column of OH ≈ Cl apatites, a second Cl site, Cl_b, is found at z ≈ 0.093, and yields bond distances to three Ca2' atoms of 2.777Å. An additional site occurs at z ≈ 0.163. Like the ClOH site in OH-Cl apatites with OH > Cl, this site (also labeled ClOH) accommodates *both* Cl and OH, with an OH occupant bonding to Ca2 at a distance of 2.404Å and a Cl occupant bonding to the disordered Ca2' atom at a distance of 2.647Å. Thus, through the disordering of Ca2 to Ca2', as in OH > Cl apatite a single site can accommodate either column anion with acceptable bond distances.

A final site, OH_a, is also present in the OH - Cl binary anion column wherein OH ≈ Cl. That site, at (0,0,1/4), is at a position in the center of the Ca2 triangle, identical to the position occupied by F in fluorapatite and ternary apatites. In their study of OH-Cl apatites, Garcia-Tunion (2012) found the OH to occupy that site as well, demonstrating that the hydroxyl can occupy the site on the mirror plane that is normally occupied by F. Bond distances from the OH

site at (0,0,1/4) to the three Ca2 atoms in the Ca2 triangle are 2.351Å, affording an acceptable (H)O-Ca bond distance.

The site occupied by OH at (0,0,1/4) was a surprise in the structure solutions, as that is a site typically only occupied by F in the apatite anion column, but in retrospect the reason for its existence is obvious. As seen in Figure 6, the OH_a site is essential for reversing the anion column. Without that site the two adjacent column-reversing sites would be occupied by a ClOH below the plane and a ClOH site above the plane, moving down the anion column. These sites would be 2.28Å apart without the intervening OH_a site, illustrating the structural role of the OH_a site, a novel OH site in the calcium phosphate apatites.

Finally, to further test the veracity of the structure model and the quality of the structure refinements, we noted that, for the structure model with OH ≈ Cl and OH > Cl, there should be a relationship between the amount of the disordered Ca2' *vs*. the amount of Cl in Cl_b plus the Cl in the ClOH site (Table 6). Because each Cl atom in Cl_b and each Cl atom in the mixed-occupancy ClOH site (calculated as noted previously) bonds to three Ca2'atoms in the disordered Ca2 triangle, we plotted the occupancy of (Ca2'/3) *vs*. (Cl_b + Cl in ClOH). Figure 7 illustrates the relationship, and the R^2 value of 0.9906 underscores the veracity of the model and the remarkable quality of the structure data, particularly considering the relatively small occupancy of the several column anion sites.

HYDROGEN BONDING IN THE ANION COLUMN

One important aspect to consider when defining the nature of column anion substitution in the apatite structure, where OH is involved, is hydrogen bonding (H-bonding). It is expected (and has been observed in the F-OH binary; Young et al. 1969) that the H associated with the OH in the anion column will form linear strong hydrogen bonds with the neighboring anions in the anion column. Furthermore, as mentioned in previous sections, H-bonding between neighboring column anions is considered essential for the existence of some of the proposed anion-anion distances. The multiple column anion sites observed in each of the three column site arrangements found when OH > Cl, Cl > OH and OH ≈ Cl, combined with many feasible arrangements of these column anion sites, leads to a large number of possible H-bonding environments in the structure of OH-Cl apatites. Table 7 lists all possible O(H)-X distances (X = OH, Cl) distances for Cl > OH (Table 1), OH > Cl (Table 3), and OH ≈ Cl (Table 5). Whereas all of the H-bonding environments are considered feasible in Table 7, they may not all actually exist. As mentioned previously in the text, in the OH ≈ Cl column site variation OH is predicted to occupy the Cl_a and Cl_b sites in a sequence necessary to incorporate Cl at the Cl_a site (Figure 6), thus H-bonding environments are included in table 7 that are a result of this necessary sequence.

Figure 8 depicts the IR spectrum in the OH stretching region of an apatite in our OH ≈ Cl compositional group (≈3550cm^{-1}). As shown therein, and also noted in spectra of Cl-OH apatites with OH > Cl and Cl > OH, there are multiple peaks in the region; the multiple peaks result from the multiple H-bonding environments for the hydroxyl hydrogens. We are currently collecting IR spectra to correlate individual absorption peaks with the individual H-bonding environments in the Cl-OH binary apatite anion column, and will report those subsequently.

IMPLICATIONS

Calcium phosphate apatite is the most abundant phosphate mineral, and a phase with fundamental importance in geology, agriculture, materials science, medicine and dentistry. All hard tissue of the human body except small parts of the inner ear is formed of apatite materials, indicating a remarkable link between the inorganic and organic genesis for the

mineral; apatite is among the few most common biominerals on Earth. In addition, apatite forms the foundation of the global phosphorus cycle. The importance of apatite in many disciplines, indeed in even sustaining human life as the chief source of phosphate for fertilizer, cannot be overstated. Despite the overwhelming importance of calcium phosphate apatite, it is remarkable that the details of this mineral are not well known.

This work elucidates the methods of achieving solid solution along the OH-Cl binary in calcium phosphate apatites, and illustrates the complex, compositional dependent nature of the solid solution mechanisms. It also demonstrates that detailed diffraction studies can reveal the fine details of the apatite atomic arrangement and the behavior of atoms in the apatite anion column.

ACKNOWLEDGEMENTS

Support for this work was provided by the National Science Foundation through grant EAR-1249459 to JMH and EAR-0952298 to JR. The manuscript was improved by reviews by Francis McCubbin and an anonymous reviewer, for which we are very appreciative.

REFERENCES CITED

Akella, J., Vaidya, S.N., Kennedy, G.C., (1969) Melting of sodium chloride at pressures to 65 kbar. Physical Review 185 (3), 1135–1140.

Brown, I.D. (1976) On the geometry of O-H…O hydrogen bonds. *Acta Crystallographica*, A32, 24-31.

Garcia-Tunion, E., Dacuna, B., Zaragoza, G., Franco, J., and Guitian, F. (2012) Cl-OH ion-exchanging process in chlorapatite ($Ca_5(PO_4)_3Cl_x(OH)_{1-x}$) – a deep insight. *Acta Crystallographica*, B68, 467-479.

Hughes, J.M. (2015) The many facets of apatite. Mineralogical Society of America Presidential Address. *American Mineralogist*, 100, 1033-1039.

Hughes, J.M., Cameron, M., and Crowley, K.D. (1989) Structural variations in natural F, OH and Cl apatites. *American Mineralogist*, 74, 870-876.

Hughes, J. M., Cameron, M. and Crowley, K.D. (1990) Crystal structures of natural ternary apatites: solid solution in the $Ca_5(PO_4)_3X$ (X = F, OH, Cl) system. *American Mineralogist*, 75, 295-304.

Hughes, J.M., Cameron, M., and Crowley, K.D. (1990) Crystal structures of natural ternary apatites: Solid solution in the $Ca_5(PO_4)_3X$ (X = F, OH, Cl) system. *American Mineralogist*, 75, 295-304.

Hughes, J.M., and Rakovan, J. (2015) Structurally robust, chemically diverse: Apatite and apatite supergroup minerals. *Elements*, 11, 167-172.

Hughes, J.M., Nekvasil, H., Ustunisik, G., Lindsley, D.H., Coraor, A.E., Vaughn, J., Phillips, B., McCubbin, F.M., and Woerner, W.R. (2014a) Solid solution in the fluorapatite - chlorapatite binary system: High-precision crystal structure refinements of synthetic F-Cl apatite. American Mineralogist 99, 369-376.

Hughes, J.M., Heffernan, K.M., Goldoff, B., and Nekvasil, H. (2014b) Fluor-chlorapatite, devoid of OH, from the Three Peaks Area, Utah: The first reported structure of natural fluor-chlorapatite. *Canadian Mineralogist*, 52, 643-652.

Jenkins, H.D.B., and Thakur, K.P. (1979) Reappraisal of thermochemical radii for complex anions. *Journal of Chemical Education*, 56, 576-577.

McCubbin, F.M., Mason, H.E., Park, H., Phillips, B.L., Parise, J.B., Nekvasil, H., and Lindsley, D.H. (2008) Synthesis and characterization of low-OH– fluor-chlorapatite: A single-crystal XRD and NMR spectroscopic study. *American Mineralogist*, 93, 210-216.

Mackie, P. E., and Young, R. A. (1974) Fluorine-chlorine interaction in fluor-chlorapatite. *Journal of Solid State Chemistry*, 11, 319-329.

Putnis, A. (2009) Mineral replacement reactions. In E.H. Oelkers and J. Schott, Eds., Thermodynamics and Kinetics of Water-Rock Interaction, 70, p. 87–124. Reviews in Mineralogy and Geochemistry, Mineralogical Society of America, Chantilly, Virginia.

Schettler, G., Gottschalk, M., and Harlov, D.E. (2011) A new semi-micro wet chemical method for apatite analysis and its application to the crystal chemistry of fluorapatite-chlorapatite solid solutions. American Mineralogist, 96, 138–152.

Shannon, R.D., and Prewitt, C.T. (1969) Effective ionic radii in oxides and fluorides. *Acta Crystallographica*, B25, 925-946.

Sheldrick, G.M. (2008) A short history of *SHELX*. Acta Crystallographica, A64, 112–122.

Sudarsanan, K., and Young, R.A. (1978) Structural interactions of F, Cl and OH in apatites. *Acta Crystallographica*, B34, 1401-1407.

Vener, M.V., Shishkina, A.V., Rykounov, A.A., and Tsirelson, V.G. (2013) Cl…Cl interactions in molecular crystals: Insights from the theoretical charge density analysis. *The Journal of Physical Chemistry A,* 117, 8459-8467.

Young, R.A., van der Lugt, W., and Elliott, J.C. (1969) Mechanism for fluorine inhibition of diffusion in hydroxyapatite. *Nature*, 223, 729-730.

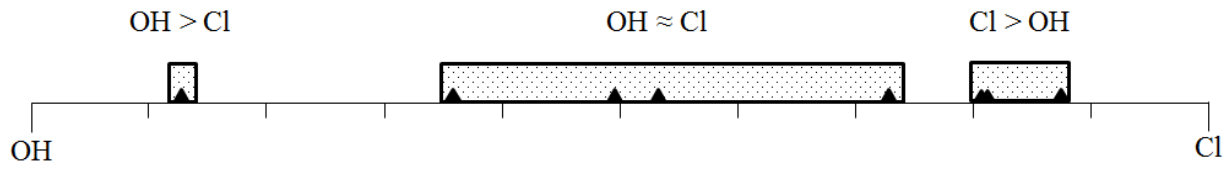

FIGURE 1. Compositions along the calcium phosphate apatite OH-Cl binary studied in this work.

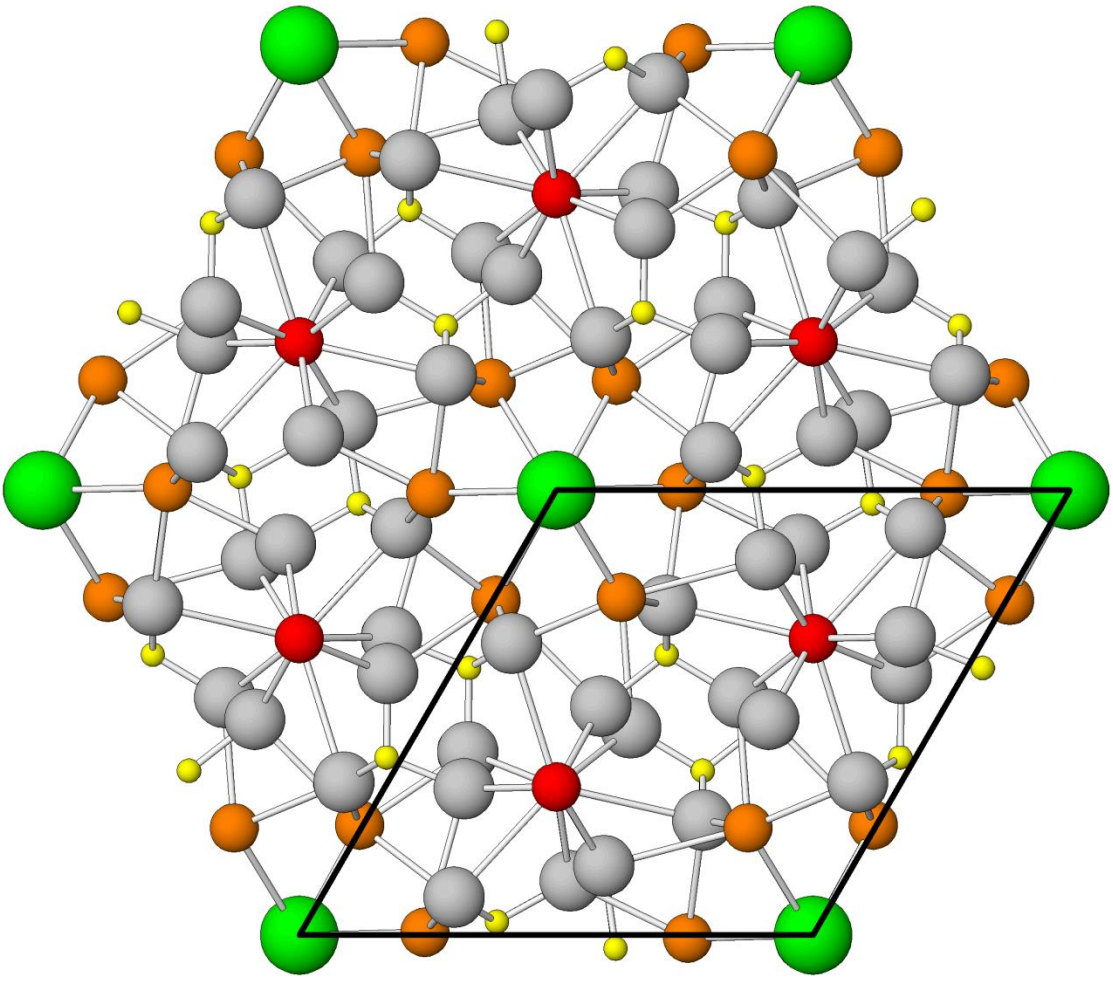

FIGURE 2. The apatite atomic arrangement projected on (001). Green atoms represent projection of anion column, yellow atoms are P, red atoms are Ca1, and orange atoms are Ca2. From Hughes (2015).

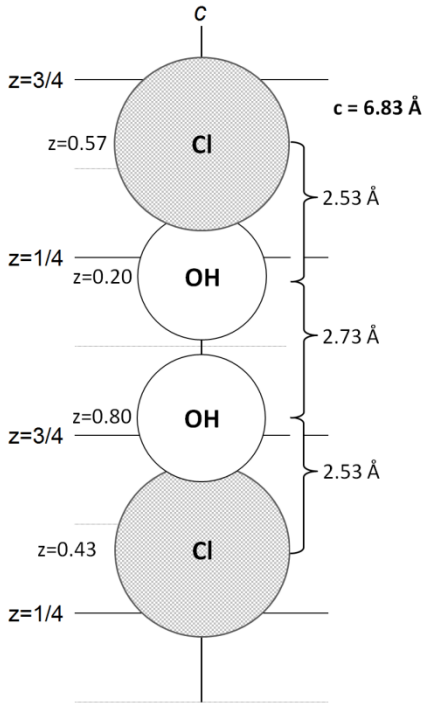

FIGURE 3. Depiction of incompatibility of OH and Cl positions observed in endmember hydroxylapatite and chlorapatite in OH-Cl binary anion column.

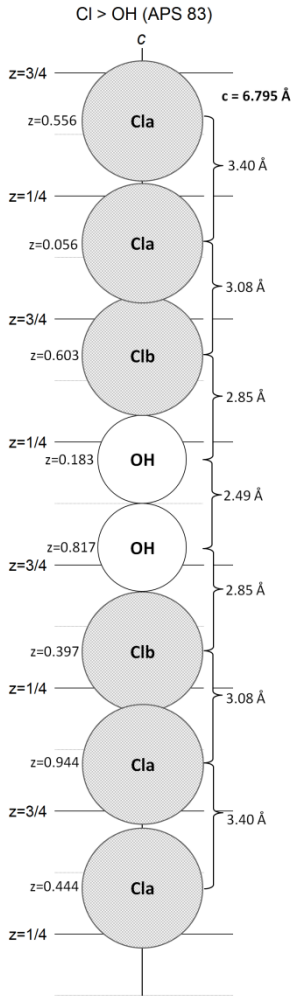

FIGURE 4. Depiction of reversal of anion column in OH-Cl binary calcium phosphate apatites with Cl > OH. The depicted sequence provides sufficient anion-anion distances and allows reversal of anion sequence to preserve $P6_3/m$ symmetry.

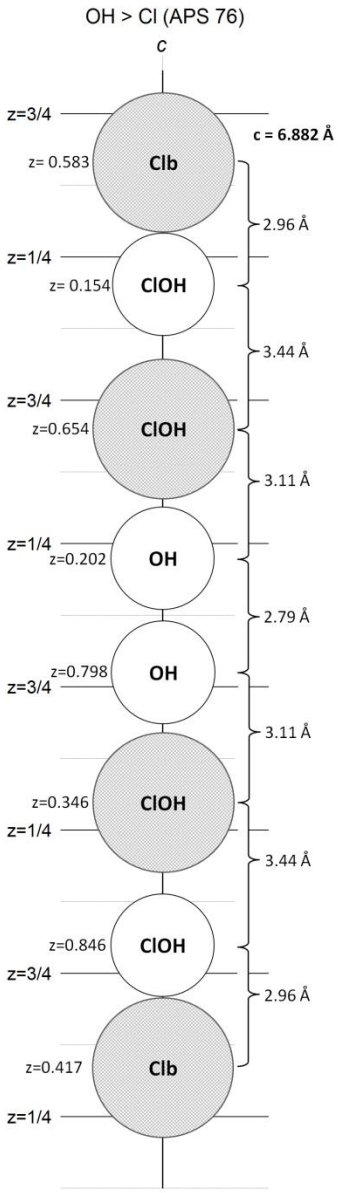

FIGURE 5. Depiction of reversal of anion column in OH-Cl binary calcium phosphate apatites with OH > Cl. The depicted sequence provides sufficient anion-anion distances and allows reversal of anion sequence to preserve $P6_3/m$ symmetry.

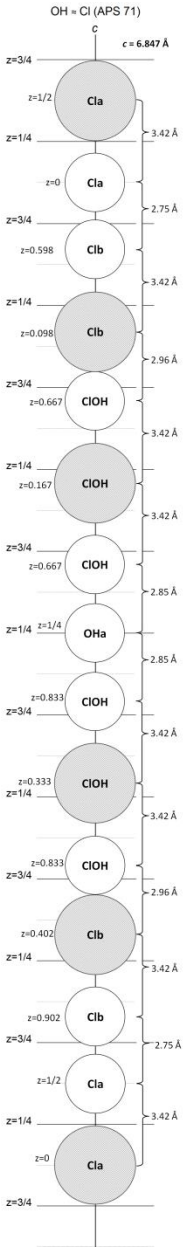

FIGURE 6. Depiction of reversal of anion column in OH-Cl binary calcium phosphate apatites with OH ≈ Cl. The depicted sequence provides sufficient anion-anion distances and allows reversal of anion sequence to preserve $P6_3/m$ symmetry.

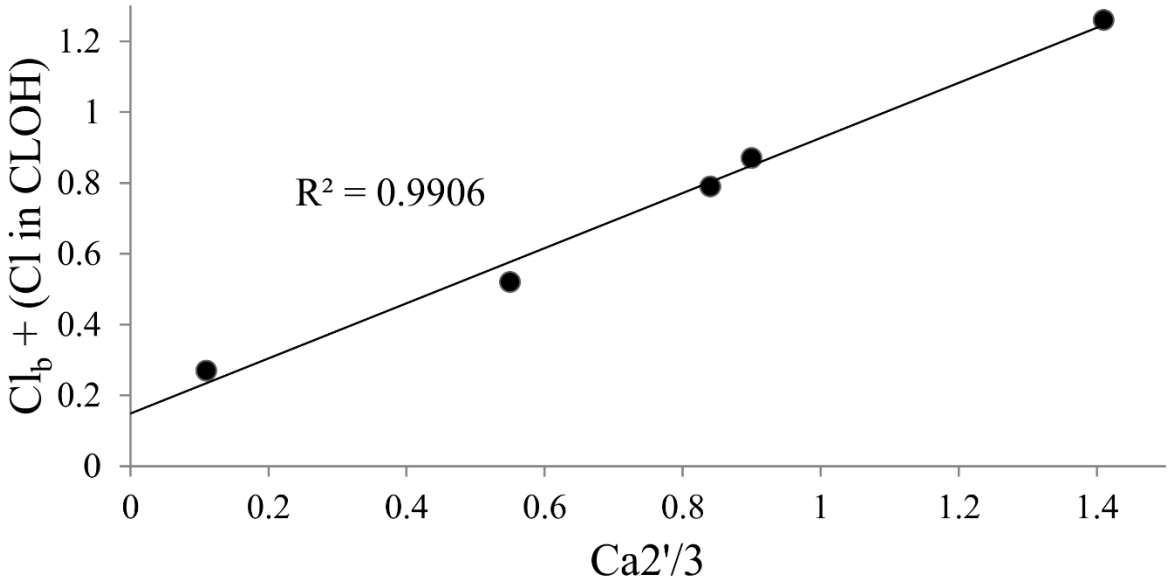

FIGURE 7. Plot of occupancy of Ca2'/3 *vs*. occupancy of [Cl_b + (Cl in ClOH)] for OH ≈ Cl apatites and OH > Cl apatites. As noted in text, because each Cl bonds to three Ca2' atoms, the relationship should be linear with an intercept of 0.

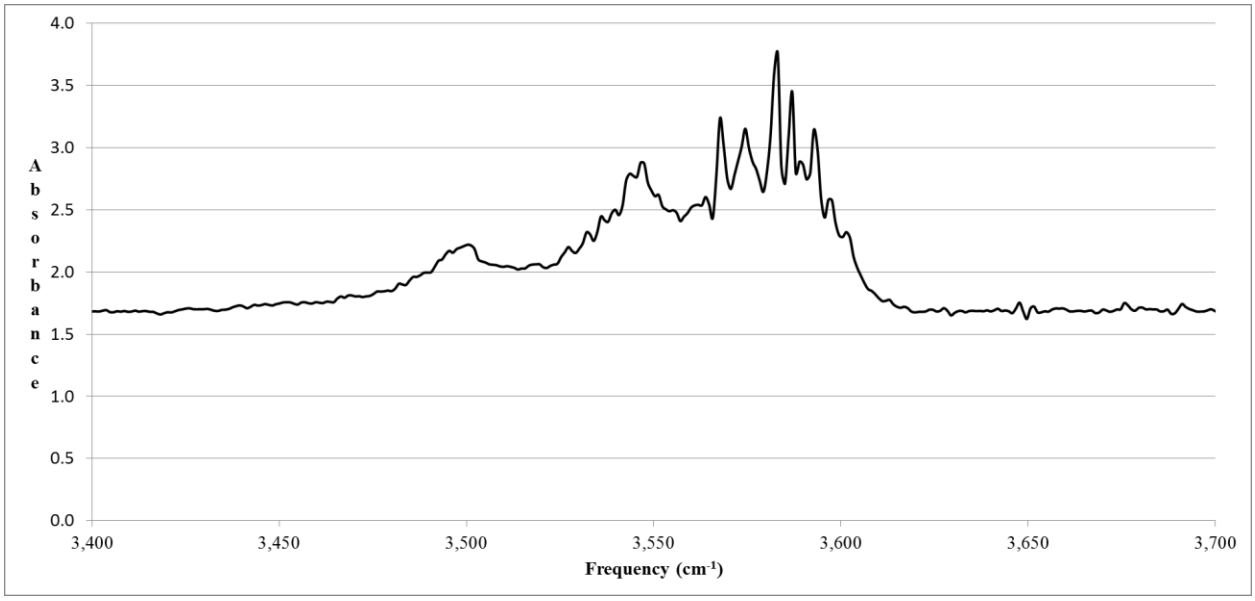

FIGURE 8. IR absorbance in the OH stretching region for APS 72. Multiple peaks are easily distinguishable, supporting the existence of many H-bonding environments in the structure of OH ≈ Cl apatites. Similar results were found for OH > Cl apatites and Cl > OH apatites.

TABLE 1. Atomic coordinates and equivalent isotropic atomic displacement parameters ($Å^2$) for sample APS83, with Cl > OH.

Atom	x/a	y/b	z/c	U(eq)*
Ca1	2/3	1/3	0.99684(5)	0.01064(8)
Ca2	0.25900(3)	0.00225(3)	1/4	0.01124(8)
P	0.62592(4)	0.03242(4)	1/4	0.00658(8)
O1	0.50913(13)	0.85072(12)	1/4	0.0133(2)
O2	0.53493(13)	0.12661(13)	1/4	0.0147(2)
O3	0.73389(10)	0.08691(10)	0.06748(13)	0.02010(18)
OH	0	0	0.183(5)	0.003(5)
ClB	0	0	0.103(3)	0.0094(16)
ClA	0	0	0.0562(8)	0.0130(6)

*U(eq) is defined as one third of the trace of the orthogonalized U_{ij} tensor.
**Total contents in unit cell.

TABLE 2. Values of *z* for column anions in (0,0,z) sites and percentage of total column anion occupancy in OH-Cl binary apatites with Cl > OH. Total sites determined by single-crystal site-refinement.

Sample	OH	% Sites	Cl_a	% Sites	Cl_b	% Sites	Column Occ.[1]
APS78	0.183	18.2	0.058	55.1	0.106	26.7	$OH_{0.37}Cl_{1.65}$
APS82	0.181	18.5	0.061	57.5	0.108	24.0	$OH_{0.38}Cl_{1.66}$
APS83	0.183	12.8	0.056	62.4	0.103	24.8	$OH_{0.26}Cl_{1.75}$

TABLE 3. Atomic coordinates and equivalent isotropic atomic displacement parameters ($Å^2$) for APS76, with OH > Cl.

Atom	x/a	y/b	z/c	U(eq)
Ca1	2/3	1/3	0.99843(5)	0.00993(8)
Ca2	0.2465(4)	0.99354(6)	1/4	0.0082(2)
Ca2'	0.275(4)	0.9922(13)	1/4	0.0082(2)
P	0.63142(4)	0.03027(4)	1/4	0.00549(8)
O1	0.51529(12)	0.84426(12)	1/4	0.01064(18)
O2	0.53517(13)	0.12240(13)	1/4	0.0140(2)
O3	0.74152(10)	0.08573(10)	0.06994(12)	0.01870(17)
OH	0	0	0.2024(14)	0.0097(10)
ClB	0	0	0.083(13)	0.092(19)
ClOH	0	0	0.154(5)	0.006(5)

*U(eq) is defined as one third of the trace of the orthogonalized U_{ij} tensor.
**Total contents in unit cell.

TABLE 4. Values of *z* for column anions in (0,0,z) sites and percentage of total column anion occupancy in OH-Cl binary apatites with OH > Cl.

Sample	OH	% Sites	Cl_b	% Sites	ClOH[1]	% Sites	Column Occ[2].
APS76	0.202	84.5	0.083	6.4	0.154	9.1	$OH_{1.73}Cl_{0.27}$

[1](ClOH site: 21.7 % OH, 78.2% Cl)
[2]Constrained to 2.00 column anions/formula unit.

TABLE 5. Atomic coordinates and equivalent isotropic atomic displacement parameters ($Å^2$) for APS71, with OH ≈ Cl.

Atom	**x/a**	**y/b**	**z/c**	**U(eq)***
Ca1	2/3	1/3	0.99776(5)	0.01068(8)
Ca2	0.2450(6)	0.9973(5)	1/4	0.0096(4)
Ca2'	0.2676(6)	0.9952(8)	1/4	0.0096(4)
P	0.62959(4)	0.03164(4)	1/4	0.00627(8)
O1	0.51273(13)	0.84771(12)	1/4	0.01273(19)
O2	0.53594(14)	0.12471(13)	1/4	0.0163(2)
O3	0.73802(10)	0.08660(10)	0.06890(13)	0.02171(19)
OHA	0	0	1/4	0.013(3)
ClOH	0	0	0.1667(9)	0.0129(10)
ClA	0	0	0	0.031(7)
ClB	0	0	0.0984(9)	0.0119(11)

*U(eq) is defined as one third of the trace of the orthogonalized U_{ij} tensor.
**Total contents in unit cell.

TABLE 6. Values of *z* for column anions in (0,0,z) sites and percentage of total column anion occupancy in OH-Cl binary apatites with OH ≈ Cl.

Sample	OH_a	% Sites	Cl_a	% Sites	Cl_b	% Sites	ClOH	% Sites	Column occ.*
APS71	1/4	19.5	0	4.2	0.098	27.4	0.167[1]	48.9	$OH_{1.01}Cl_{0.99}$
APS72	1/4	7.0	0	5.9	0.082	52.5	0.156[2]	34.5	$OH_{0.53}Cl_{1.47}$
APS74	1/4	17.7	0	4.0	0.096	30.7	0.164[3]	47.6	$OH_{0.92}Cl_{1.08}$
APS80	1/4	25.9	0	3.8	0.096	16.9	0.164[4]	53.4	$OH_{1.30}Cl_{0.70}$

[1](ClOH site: 63.0 % OH, 37.0% Cl); [2](ClOH site: 56.3 % OH, 43.7% Cl);
[3](ClOH site: 60.0 % OH, 40.0% Cl); [4](ClOH site: 72.8 % OH, 27.2% Cl).
*Constrained to (OH+Cl) = 2.00.

TABLE 7. List of the theoretical H-bonding environments that may possibly exist for each structural type, using APS 71, 76, and 83 as models. OH...O represents H-bonding to a neighboring O anion, and OH...Cl represents H-bonding to a neighboring Cl anion. The site column and the neighbor column represent the two anion sites that when placed next to each other in the column yield the corresponding anion-anion distance listed. The Cl_b – Cl_a, Cl_b – Cl_b, and Cl_a – Cl_a H-bonding environments in the OH ≈ Cl compositional range are predicted to exist, likely at low occupancy.

	O-H…O				**O-H...Cl**		
	Anion-Anion Distance (Å)	Site	Neighbor		Anion-Anion Distance (Å)	Site	Neighbor
OH ≈ Cl, APS 71	3.42	ClOH	ClOH		3.42	ClOH	ClOH
	4.56	ClOH	ClOH		4.56	ClOH	ClOH
	2.85	ClOH	OHa		3.89	ClOH	Clb
	3.99	ClOH	OHa		2.96	ClOH	Clb
	3.42	OHa	OHa		5.03	ClOH	Clb
					4.46	OHa	Clb
					3.99	OHa	ClOH
	2.75	Clb	Cla		3.42	Clb	Clb
					3.42	Cla	Cla
	O-H…O				**O-H...Cl**		
	Anion-Anion Distance (Å)	Site	Neighbor		Anion-Anion Distance (Å)	Site	Neighbor
OH > Cl, APS 76	3.44	ClOH	ClOH		3.44	ClOH	ClOH
	4.77	ClOH	ClOH		4.77	ClOH	ClOH
	3.11	ClOH	OH		3.11	ClOH	OH
	3.78	ClOH	OH		3.78	ClOH	OH
	4.43	ClOH	OH		4.43	ClOH	OH
	2.45	ClOH	OH		3.93	ClOH	Clb
	2.79	OH	OH		2.96	ClOH	Clb
	4.10	OH	OH		4.26	OH	Clb
	3.44	OH	OH		4.92	OH	Clb
	O-H…O				**O-H...Cl**		
	Anion-Anion Distance (Å)	Site	Neighbor		Anion-Anion Distance (Å)	Site	Neighbor
Cl > OH, APS 83	3.40	OH	OH		4.26	OH	Cla
	2.49	OH	OH		5.17	OH	Cla
	4.30	OH	OH		3.94	OH	Clb
					2.85	OH	Clb
					4.85	OH	Clb

Column anion arrangements in chemically zoned ternary chlorapatite and fluorapatite from Kurokura, Japan

Published in American Mineralogist volume 102 (in press), 2017

SEAN R. KELLY[1], JOHN RAKOVAN[1]
[1]Department of Geology and Environmental Earth Science, Miami University, Oxford, Ohio 45056, U.S.A.

JOHN M. HUGHES[2]
[2]Department of Geology, University of Vermont, Burlington, Vermont 05405, U.S.A.

ABSTRACT

The substitution of F, OH and Cl in apatite has recently gained increased attention due to the complex nature of incorporation of these three constituents and the implications of apatite column anion chemistry, such as apatite's contribution to the water budget of the moon and Mars and the use of apatite anion chemistry as an indicator of halogen and water activities. The solid solutions among F, OH, and Cl are complex because the end-member atomic arrangements cannot fully explain the ternary and binary substitutions of these constituents due to differing atomic radii and the resulting steric constraints in the structure. Three structural variations have recently been reported for the OH-Cl binary solid solution in synthetic samples. This study elucidates column anion arrangements in a chemically zoned ternary apatite from Kurokura, Japan. The structures of the compositionally different core and rim were solved (R1=0.0158 and R1=0.0143, respectively) in space group $P6_3/m$ using single crystal X-ray diffraction data. The chemistry of these apatites was analyzed using electron microprobe analysis and crystal structure refinement. The core of the Kurokura crystal is a naturally occurring example of the OH ≈ Cl apatite structural variation in a ternary chlorapatite, with four column anion sites (one for F, two for Cl and one for *both* OH and Cl). The rim exhibits a previously unseen apatite structural variation in a ternary OH-rich fluorapatite (with only a trace Cl component) with three column anion sites (one each for F, OH and Cl). Both structural variations show a splitting of the Ca2 site that enables reasonable column anion bond distances with Ca2 atoms. A sequence of anions that provides reasonable anion-anion distances while simultaneously enabling reversal of the anion sites relative to the mirror planes at $z = 1/4$ and $z = 3/4$ exists for both structure variations. This study demonstrates the structural complexity of natural ternary apatites, and that a structural variety of OH-Cl apatite occurs over a wider range of chemistry than initially anticipated. The results have implications regarding the poorly understood (and potentially complex) crystallization history of apatite from Kurokura, Japan.

Keywords: apatite, ternary solid solution, chlorapatite, Kurokura, Japan

INTRODUCTION

Apatite *sensu lato* [$Ca_{10}(PO_4)_6(OH,F,Cl)_2$; OH = hydroxylapatite, F = fluorapatite, Cl = chlorapatite], the most abundant phosphate mineral on Earth, plays an important role across many disciplines (Hughes and Rakovan 2002; Hughes and Rakovan 2015; Rakovan and Pasteris 2015). Hydroxylapatite is the closest naturally occurring analog to bone material, and new insights about the occurrence of OH in bone apatite have recently been reported (Pasteris et al.

2014). Apatite is also one of the more common hydroxyl-bearing phases in extraterrestrial systems, such as the moon and Mars (McCubbin and Jones 2015; McCubbin et al. 2010a; Boyce et al. 2010). Boyce et al. (2014) recently suggested that apatite plays the dominant role in fractionation of F, OH, and Cl in lunar magmatic systems. Understanding the structure and thermodynamic properties of apatite will allow better estimation of the overall H_2O content within extraterrestrial magmatic systems from measured apatite chemistries.

The F, OH, and Cl chemical variation in apatite can also provide a variety of geochemical information. One example is using apatite anion chemistry as a geothermometer (*e.g.*, Stormer and Charmichael 1971). Apatite anion chemistry can also serve as an indication of magma or aqueous fluid composition from which the phase crystallized (Piccoli and Candela 2002), including the fugacity of volatiles in magmatic, metamorphic, or hydrothermal systems (Webster and Piccoli 2015; McCubbin et al. 2015; Hughes et al. 1990; Yardley 1985).

Chlorapatite, an uncommon naturally occurring apatite phase, is unique in that it can indicate rather unusual mineralization environments where it is found. For example, experimental work has suggested that Cl-rich apatite may be chemically associated with Pt in mineralizing hydrothermal fluids, demonstrating the significance of apatite anion chemistry to mineral exploration (Webster and Piccoli 2015).

As noted by Hughes et al. (2016), for any combination of anion occupants, the positions of the anions in the [0,0,*z*] anion column result from several factors, including the size of the particular column anions, the nearest-neighbors in the anion column and electrostatic repulsions therefrom, any dissymmetrization (lowering of crystal symmetry) that is present in the structure, electrostatic attractions to the surrounding triangle of Ca2 atoms, and, in hydroxyl-bearing apatite, the hydrogen bonding that occurs from the hydroxyl hydrogen to neighboring column anions. Figure 1 shows a [001] projection of the apatite atomic arrangement. Because of the steric flexibility of its structure, apatite can incorporate a large range of (F, Cl, OH) compositions in the anion column sites.

Hughes et al. (1989) published one of the most recent structural analyses of the OH, F, and Cl end members of the ternary system of anion substitution. Apatite most commonly crystallizes in space group $P6_3/m$, although subsymmetric varieties are known (Hughes and Rakovan 2015). In end-member fluorapatite, the F anion resides at (0, 0, 0.25) and (0, 0, 0.75) in the unit cell, lying on {001} mirror planes at $z = 1/4$ and $z = 3/4$. The larger OH and Cl (poly)anions are usually displaced off this mirror plane (*ca*. 0.3 and 1.3Å, respectively), a structural response to steric interaction with the surrounding Ca cations (the Ca2 position, see Figure 1), which also lie on the mirror planes. Figure 1 demonstrates the configuration of calcium anions surrounding the column anion. Although the substitution of these three anions is known to be extensive, the continuous solution series of these anions cannot be explained by their end-member atomic sites alone (Hughes et al. 1990).

It has been shown that novel, non-end member atomic sites exist in the ternary solution series as well as the binary F-Cl and OH-Cl solution series (Hughes et al. 1990, 2014a, 2014b, 2016). Hughes et al. (1990) also demonstrated in natural samples that ternary solid solution can occur *via* ordering of OH and Cl atoms, causing symmetry reduction to $P2_1/b$. The F-OH apatite binary can exist with the end-member F and OH sites while maintaining $P6_3/m$ symmetry, as the smaller radii of these (poly)anions enable disorder about the mirror planes without necessitating new sites (Hughes et al. 1989). Hughes et al. (2016) recently demonstrated, in a series of synthetic apatites, that three different structures with distinctly different column anion sites enable solid solution along the OH-Cl binary series without reduction of symmetry due to

ordering. The structure of OH-Cl apatites is influenced by column anion chemistry, with one arrangement for apatites with OH dominant, one for apatites with approximately equal OH and Cl *apfu*, and one for apatites with Cl dominant in the anion column. The calcium phosphate apatite structure preferentially incorporates F over both OH and Cl (Boyce et al. 2014). In order for natural apatite dominated by OH and Cl to exist, crystal growth must have occurred from a fluid or magma substantially devoid of F relative to OH or Cl. This study presents the structure and chemistry of a natural Cl- and OH-dominant calcium phosphate apatite from Kurokura, Ashigarakami district, Kanagawa Prefecture, Japan, and an analysis of the column anion arrangement. These apatites occur in hydrothermal veins in diorite and granodiorite, in association with quartz, chlorite, talc, stilbite, and natrolite. Crystals are prismatic with well-developed {100} {001} {101} faces and are typically 0.5-1.0 cm in length, but can exceed 4 cm (Figure 2). Apatites from Kurokura were first reported to be chlorine dominant by Harada (1938). Apatites from this locality consist of two visually distinct concentric zones: a volumetrically dominant clear core and a white (cloudy) rim (Figure 2). The rim is cloudy due to a high density of small fluid inclusions (note: the larger 'bubbles' in this image occur in the epoxy rather than the mineral; the fluid inclusions in the rim are much smaller). Harada (1938) demonstrated both optically and with wet chemical analysis that the cloudy rim and clear core represent two distinct apatite chemistries. Apatite from the core is more Cl rich than that from the rim. This concentric chemical zoning may be indicative of variation in source fluid chemistry during apatite crystallization, or possibly post-growth alteration of the rim. Although the chemical analysis of Harada (1938) suggests that both the core and rim contain significant F, preliminary investigation in this study suggested that one or both of these phases is OH-rich chlorapatite.

EXPERIMENTAL

Single crystal x-ray diffraction (SCXRD) was used as a crystal structure analysis technique and chemical probe of the apatite samples from Kurokura in this study. There are some instances, however, where different anions are shown to occupy the same column site (Hughes et al. 2014a, 2016), causing a limitation in the accuracy of this methodology. Electron microprobe analysis (EMPA) was employed as a complementary technique for analysis of the F and Cl chemistry. Measuring O with EMPA is known to be problematic; OH chemistry is instead calculated by difference, assuming two column (poly)anions per unit cell. This method of determining OH chemistry is not ideal, particularly given the known limitations of measuring F and Cl by microprobe analysis (discussed below).

Electron microprobe analysis

A sample of Kurokura apatite was prepared for EPMA analysis by embedding the crystal in epoxy resin and slicing to achieve a (100) section. The sample was then progressively polished down to a 0.02 μm alumina paste. Measuring the Cl and F composition of apatite using EPMA is known to be problematic (Stormer et al. 1993; Stock et al. 2015), as column anion migration can lead to spurious results. One way to reduce column anion migration is to use (100) sections for analysis (Stormer et al. 1993). Six spots were measured on the polished sample, three within the clear core and three within the white rim.

Compositional analyses were acquired on a Cameca SX100 electron microprobe, at the University of Oregon's CAMCOR MicroAnalytical facility, equipped with 5 tunable wavelength-dispersive spectrometers. A 15 keV accelerating voltage and 20 nA beam current

were used for measurement of Ca, F, Cl, P, and Fe, and a 20 keV accelerating voltage and a 50 nA beam current were used for measurement of S, Nd, Na, Sr, Ce, Mn, Si, Dy, and Eu. The beam size was 10 microns for all analyses. Elemental analyses were acquired using the following analyzing crystals: LIF (Fe, Dy, Eu), PET (Ca, S, Nd, Si, P), LPET (Ce, Mn, Cl), and LTAP (Sr, F, Na). The standards used were synthetic MnO (Mn), SrTiO3 (Sr), synthetic chlorapatite (halogen corrected) (P, Ca, Cl), nepheline (partial anal.) (Na, Si), magnetite (Fe), pyrite (S), BaF_2 (F), $CePO_4$ (Ce), $DyPO_4$ (Dy), $EuPO_4$ (Eu), and $NdPO_4$ (Nd). The counting time was 60 seconds for F, Cl, Fe, S, Nd, Na, Sr, Ce, Mn, Dy, and Eu, 90 seconds for P and Ca, and 120 seconds for Si. The intensity data were corrected for time dependent intensity (TDI) loss (or gain) using a self-calibrated correction for Ca, F, Cl, P, and Fe. This correction accounts for the known variation of F and Cl peak intensity over time in apatite due to anion migration. The off-peak counting time was 30 seconds for Ca and P, 60 seconds for Cl, F, Fe, S, Nd, Na, Sr, Ce, Mn, Dy, and Eu, and 120 seconds for Si. Interference corrections were applied to F (P, Ce, Eu and Nd), Cl (Nd), Nd (Ce and Eu), Sr (Si), Ce (Sr), Mn (Nd and Eu), Dy (Mn, Eu, and Fe), and Eu (Mn and Nd). Oxygen was calculated by cation stoichiometry and included in the matrix correction. Oxygen-equivalence from halogens (F/Cl/Br/I), was not subtracted in the matrix correction. Hydrogen was calculated by difference. Further details of the EMPA experimental methods used in this study can be found in Armstrong (1988) and Donovan et al. (1993; 2011).

Single crystal X-ray diffraction

X-ray diffraction data were collected with a Bruker Apex II CCD single-crystal diffractometer using graphite-monochromated Mo K_α radiation. For each sample, redundant data were collected for a sphere of reciprocal space (4,500 frames, 0.20º scan width, average redundancy ≈ 16) and were integrated and corrected for Lorentz and polarization factors and absorption using the Bruker Apex2 package of programs. The atomic arrangement was refined in space group $P6_3/m$, on F^2, with SHELXL-97 (Sheldrick 2008) using neutral atom scattering factors and full-matrix least-squares, minimizing the function $\Sigma\, w(F_o^2 - F_c^2)^2$ with no restraints. All atoms were refined with anisotropic temperature factors except the column anions. As noted previously (e.g., Hughes et al. 1990a, 2014a, 2016) use of anisotropic atomic displacement factors for the column anions yields unreasonable values of U_{33}, an anisotropy that masks the positions of anion sites occupied by small fractions of a column anion. The occupancy values of the column anions were not constrained.

After structure solution and initial refinement, the column anion positions were analyzed by difference maps. In this way, positions along the anion column were modeled and refined one at a time, as they sequentially appeared as the highest peaks in the difference maps. Disorder of the Ca2 site was also modeled in this fashion, as sites Ca2 and Ca2'. When disorder of the Ca2 site was modeled, the sum of the Ca2 and Ca2' site occupancy was constrained to total 1.00 and the two sites were also constrained to have identical thermal parameters. An extinction coefficient was also refined in both samples. Using previous literature, anion positions were named and assigned an anion scattering factor (Cl, O, or F). Anion selection was then evaluated using the calculated total anion *apfu* based on the refinement.

RESULTS

Electron microprobe analysis

Table 1 shows the chemistry results from EMPA data for each portion of the crystal. Figure 3 shows the column anion chemistry results from each of the six individual analysis spots, as well as average anion chemistry for the core and two averages for the rim. The average core anion chemistry is $[Cl_{0.93}\ (OH)_{0.66}\ F_{0.38}]$ and the average rim anion chemistry is $[F_{0.97}\ (OH)_{0.88}\ Cl_{0.24}]$. As determined by Harada (1938), the apatite core has a higher Cl concentration than the rim. Figure 3 demonstrates a notable presence of column anion chemical heterogeneity in the Kurokura apatite, particularly in the rim. One of the three spots where rim chemistry was measured has anion values much more similar to the core than the other two rim spots (Figure 3; see labeled outlier spot). Although this may simply represent heterogeneity in the rim, the outlier may also be the result of collecting data across the boundary between the core and rim. Because of this possibility, an average rim chemistry from EMPA analysis not including the outlier is also shown in Figure 3. Comparison of EMPA data to anion chemistry determined by crystal structure analysis is given below.

Crystal structure refinements

The structures of the clear apatite core and cloudy rim were solved and refined using SCXRD data to R1 values of 0.0158 and 0.0143, respectively. Both samples were successfully modeled in space group $P6_3/m$. Tables 2 and 3 contain the atomic coordinates and equivalent atomic displacement parameters for the core and rim, respectively. From the refined atomic arrangement, the core anion chemistry is $[Cl_{0.87}\ (OH)_{0.58}\ F_{0.55}]_{\Sigma 2.00}$ and the rim apatite's chemistry is $[F_{1.05}\ (OH)_{1.02}\ Cl_{0.04}]_{\Sigma 2.12}$. These results are plotted on Figure 3, alongside the results from EMPA. There is some disagreement between anion chemistry determined by SCXRD and EMPA, primarily for the rim sample. This difference may be the result of analytical error, particularly with EMPA due to the known limitations in quantifying F and Cl (and the inability to measure OH). The discrepancy may also be in part due to heterogeneity in the samples; the data from EMPA and SCXRD were collected on different individual crystal fragments.

The clear core has the same column anion arrangement reported in Hughes et al. (2016) that exists for OH-Cl apatites with OH occupancy approximately equal to Cl occupancy in the anion column. Conversely, the cloudy rim was found to have a new column anion arrangement for ternary apatites that are predominantly F and OH. The column anion arrangements of each zone of the crystal are discussed further below.

Clear apatite core

Four anion column sites were refined for the sample of the clear core portion of the Kurokura apatite, yielding a column anion arrangement almost identical to the Cl ≈ OH apatite structure published in Hughes et al. (2016). The position and occupancy of the four sites are given in Table 4.

Two distinct Cl sites were found at $z = 0$ and $z = 0.094$. The site at $z = 0$ represents a unique Cl position only found in binary F-Cl and OH-Cl calcium phosphate apatites (Hughes et al. 2014; 2016). The site at $z = 0.094$ is nearly equivalent to the Cl atomic site in end-member chlorapatite, only slightly less displaced from the mirror planes at $z = 1/4$ and $z = 3/4$ than the typical end member Cl site ($z \approx 0.068$; Hughes et al. 1989). This site has an acceptable bond distance to Ca2' of 2.878Å.

Another column anion site was found in the clear apatite core samples at $z = 0.166$. This site is particularly interesting, having only recently been documented in Hughes et al. (2016). As

is the case in Hughes et al. (2016), here it is demonstrated that this site represents a special site with mixed occupancy of *both* OH and Cl.

In order for OH and Cl (poly)anions with significantly different radii (Cl = 1.72Å, OH = 1.33Å; Jenkins and Thakur 1979) to occupy the same atomic site, they must both achieve acceptable bond distances with the neighboring Ca2 site. This requires the splitting of the Ca2 site into two distinct sites, which was found in this structure refinement (Ca2 and Ca2'; Table 2). The ClOH site has a distance of 2.387Å to the Ca2 site (acceptable for OH) and 2.637Å to the Ca2' site (acceptable for Cl). These interatomic distances are almost identical to those found in Hughes et al. (2016) (2.404Å to Ca2 and 2.647Å to Ca2'). Further supporting mixed occupancy of the site at $z = 0.166$ is that the sum of the site occupancies of the column anions (which should be approximately 2 anions per unit cell) is substantially *below* 2.00 when the ClOH site is modeled as Cl (1.70 atoms per unit cell) and substantially *above* 2.00 when the ClOH site is modeled as OH (2.39 atoms per unit cell). Because of this, as in Hughes et al. (2016), a total column occupancy of 100% (2.00 atoms per unit cell) was used to calculate the proportion of the ClOH site occupied by each anion (Table 4).

A final site was found at $z = 1/4$, directly centered among three Ca2 cations on the mirror plane at $z = 1/4$ and $z = 3/4$ and concordant with the F position in end-member fluorapatite. However, Hughes et al. (2016) found that in their synthetic apatite where OH ≈ Cl (with anion sites identical to those published here) OH can occupy this site. Dual occupancy of this site by F and OH makes fractional occupancy determination *via* SCXRD difficult, because the scattering factors of O^{2-} and F^{-} are nearly identical as they are isoelectronic. However, EMPA data from the Kurokura core (Table 1; Figure 3) indicates 16-23% F occupancy of the anion column. This occupancy coincides closely with the refined site occupancy at $z = 1/4$ in the structure (28% occupied, Table 4), suggesting that this site is exclusively (or almost exclusively) occupied by F in the Kurokura core. No OH was modeled at this site in the refinements. This demonstrates that the OH ≈ Cl apatite structural result found in Hughes et al. (2016) occurs over a wider range of apatite anion chemistry than just in the OH-Cl binary, and that this structure variant, i.e. column anion arrangement, is found in nature.

For this apatite sample to maintain the hexagonal symmetry of space group of $P6_3/m$, it must be demonstrated that a sequence of atoms exists, given the refined atomic sites in the anion column, to reverse the ordering of sites from above the mirror planes at $z = 1/4$ and $z = 3/4$ to below these mirror planes, such that throughout the crystal the occupancies are averaged half above and half below. Hughes et al. (2016) proposed a model for reversal of the anion column with acceptable anion-anion distances for this particular apatite structure. This model is shown in Figure 4, with the only difference being F occupancy of the site at $z = 1/4$ and 3/4. The *c* dimension of the structure from this paper is only 0.002 Å larger than that used in the model from Hughes et al. (2016), and the interatomic distances are effectively identical. As mentioned in Hughes et al. (2016), OH must occupy the Cla and Clb site in trace quantities to enable this reversal sequence. Given the constraints proposed in Mackie and Young (1974): (1) the interatomic distances between occupants of the anion column must be of reasonable length, 2) the anions must occupy positions found in the structure refinement, and 3) F [and OH] can occupy a Cl site but Cl cannot occupy an F [or OH] site because of the resulting short Ca-Cl distances, it is reasonable to propose that *both* F and OH can occupy the Cla and Clb sites (F and OH are both smaller than Cl), making reversal of the anion column *via* the sequence in Figure 4 possible.

White apatite rim

The structure of the white outer rim of the apatite crystal (Figure 2) was found to have three column anion sites, with the overall chemistry being that of a OH-rich fluorapatite (almost identical OH and F concentrations) with a small chlorine component. The unit cell fractional coordinates of these column anion sites and their occupancy factors are given in Table 5.

One column anion site was modeled at $z = 1/4$, identical to the end-member fluorapatite column site. This site is considered here to be occupied by F, as with the core refinement there is no reason to suggest it is occupied by OH. The EMPA data demonstrate high F in the apatite rim (Table 1), supporting the occupancy of the $z = 1/4$ site by F. Another site was refined at $z = 0.19$. This was modeled as an OH site, as it is close to the end-member hydroxylapatite column site ($z \approx 0.20$, Hughes et al. 1989). A third site was modeled at $z = 0.11$, which is slightly less offset from the mirror planes at $z = 1/4$ and $z = 3/4$ than the end-member chlorapatite site ($z \approx 0.068$). This site was modeled as a Cl site.

A splitting of the Ca2 site into Ca2 and Ca2' was also modeled in this sample. The F and OH sites have acceptable bond distances to the Ca2 site of 2.32Å and 2.35Å, respectively. The Cl site is prohibitively close to the Ca2 site (2.51Å), but has an acceptable bond distance of 2.79Å to the Ca2' site, making the Ca2' site a necessary component of this apatite structure. The short Ca2' to O2 distance (2.11 Å) indicates the requirement of an O2' site for the Ca2' site to be feasible. The highest peak in the difference map (0.51 $e^-/Å^3$) is an O2' site that when modeled provides an acceptable Ca2'-O2' distance (2.39 Å), affirming the O2 disorder. However, the data could not successfully support the modeling of disordered O2 and the concomitant disordering of P, and thus it was not modeled.

The combined column anion site occupancy refined to 2.12 sites per unit cell, slightly over the 2.00 sites per unit cell mandated by the apatite structure. This indicates a potential inaccuracy in the refinement. One possible explanation for the over occupancy of the anion column in the rim refinement is that there is Cl occupying the OH or F site that is not being accounted for in the model. The interatomic distances between the Ca2' site and the F/OH sites (Ca2'-OH: 2.66Å; Ca2'-F: 2.63Å) are both large enough to ideally accommodate Cl. This suggests that there may be a small amount of Cl occupancy in either (or both) the F and OH sites (more likely the OH site) that is accounting for the over occupancy of the anion column in the model. Adding Cl occupancy at the F and OH sites moves the SCXRD anion chemistry closer to the anion chemistry determined by EMPA, as EMPA found substantially more Cl than SCXRD (2.1% vs. 12% of total column occupancy, respectively). However, the very small occupancy of the Ca2' site (3.49% occupied) suggests that only a very small amount of substitution of Cl into the OH or F sites may be occurring, if any. As mentioned in Hughes et al. (2016), there should be a 1:1 linear relationship between the occupancy of the Ca2' site and the occupancy of the column anion sites that require the Ca2' site to have reasonable bond distances. The Cl site in this structure is 2.12% occupied, leaving 1.37% possible occupancy of the F and OH sites by Cl.

This apatite column anion arrangement has not previously been documented. However, comparison below demonstrates that the structure may represent a low Cl analog to the hexagonal structure of a ternary apatite collected from "ash F" in the Gunnison Formation near Jackson Peak, southwestern Utah, published in Hughes et al. (1990). That structure has identical F and OH sites, as well as splitting of the Ca2 site (with a short 2.16Å Ca2'-O2 distance). The only structural difference is that, unlike the structure published here, Hughes et al. (1990) documented a splitting of the Cl site into two: one at $z = 0.132$ and another at $z = 0.06$. Splitting of the Cl site was proposed due to the abnormally large U_{33} value (0.098Å). The U_{eq} value for the

Cl site in the rim structure in this paper is not unusually large (0.01045), and thus a split is not considered. A key difference that likely explains this observation is the different chemistry of these apatites.

The apatite described herein is approximately a pure binary F-OH apatite, with only 0.04 Cl atoms per unit cell. The small occupancy on the Cl site in this structure provides uncertainty as to the legitimacy of the site. The site was included in the model, however, due to EMPA data showing substantial Cl, the presence of the Ca2' site, and that removal of the Cl site from the refinement leads to a higher R value (0.0149) and the appearance of an electron density peak of 0.64 $e^-/Å^3$ in the difference map near $z = 0.10$ (near the Cl site).

The ternary apatite from Hughes et al. (1990) has a much higher Cl occupancy of 0.63 Cl atoms per unit cell. The greater proportion of Cl in the apatite from Hughes et al. (1990) may be what causes the splitting of the Cl site. Furthermore, a greater Cl occupancy can also make it easier to resolve a splitting of the Cl site. The very low Cl occupancy of the Kurokura rim structure is effectively a limitation in observing this split if it does exist.

A model demonstrating a possible reversal of the column anion occupancy necessary to maintain $P6_3/m$ symmetry using the sites found in this study is shown in Figure 5. As seen in Figure 5, the most prohibitive anion-anion distance necessary to enable disorder of anion sites from one side of the mirror plane at $z = 1/4$ and $z = 3/4$ to the other is an OH-Cl distance of 2.89Å. This distance is greater than an OH-Cl distance proposed in Hughes et al. (2016) (2.85Å), and is considered acceptable.

IMPLICATIONS

This study presents two structural variations of apatite, within compositionally different concentric zones of the same crystal, which have previously not been documented in natural samples. Whereas a naturally occurring OH-Cl binary apatite was not found, the clear core portion of these apatite crystals represents the first naturally occurring example of the OH ≈ Cl OH-Cl apatite structure variety first published in Hughes et al. (2016). The fact that this structure was found in an apatite with a significant F component demonstrates that this structural result occurs over a wider range of apatite chemistries than documented in Hughes et al. (2016) using pure Cl-OH synthetic crystals. The rim represents an F- and OH-dominant ternary apatite with a new structural variety closely resembling previously documented hexagonal ternary apatite (Hughes et al. 1990).

The distinct difference in chemistry from the core and rim suggests that the two zones of the crystal represent either two distinct mineralization events/fluids or one mineralization event that was later metasomatically altered. The rim representing an alteration phase is consistent with the substantial chemical heterogeneity of the rim observed in the microprobe data (Figure 3).

Further investigation will be necessary for addressing the petrological questions posed herein. New analyses, such as an elemental map documenting the chemistry variation over a section of a crystal, or analysis of the fluid inclusions present in the rim, may elucidate the cause of the anion chemistry variation from the rim to the core. Understanding the petrogenic history of this apatite is pertinent to the interpretation of these results from a petrological standpoint. It is possible that the two different apatite structural varieties presented here are affected both by variation in chemistry (evident given the difference in anion chemistry in each phase) and variation in temperature, particularly given the possibility that the rim may represent a lower temperature alteration of the original apatite phase.

There is little background literature on the crystallization events of the Kurokura region, making it impossible to put the work of this paper into the context of the greater geology of Kurokura. Further studies of this region will help to better characterize the unique formation conditions responsible for formation of apatite at Kurokura.

ACKNOWLEDGEMENTS

Support for this work was provided by the National Science Foundation through grant EAR-1249459 to JMH and EAR-0952298 to JR. Reviews by Francis McCubbin, Jill Pasteris, and an anonymous reviewer improved this manuscript significantly.

REFERENCES

Armstrong, J.T. (1988) Quantitative analysis of silicate and oxide materials: comparison of Monte Carlo, ZAF, and phi-rho-z procedures. Microbeam Analysis, 239-246.

Boyce, J.W., Liu, Y., Rossman, G.R., Guan, Y., Eiler, J.M., Stolper, E.M., and Taylor, L.A. (2010) Lunar apatite with terrestrial volatile abundances. Nature Letters, 466, 466-469.

Boyce J.W., Tomlinson S.M., McCubbin, F.M., Greenwood, J.P., and Treiman, A.H. (2014) The Lunar Apatite Paradox. Science, 344, 400–402.

Donovan, J.J., Lowers, H.A, and Rusk, B.G. (2011) Improved electron probe microanalysis of trace elements in quartz. American Mineralogist, 96, 274–282.

Donovan, J.J., Snyder, D.A., and Rivers, M.L. (1993) An Improved Interference Correction for Trace Element Analysis. Microbeam Analysis, 2, 23-28.

Harada, Z. (1938) Beiträge zur Kenntnis der optischen und chemischen Eigenschaften de Apatits von Kurokura, Kanagawa Präfektur. Journal of the Faculty of Science, Hokkaido Imperial University. Ser. 4, Geology and mineralogy, 4, 11-16. (in German)

Hughes, J.M., and Rakovan, J. (2002) The Crystal Structure of Apatite, $Ca_5(PO_4)_3(F,OH,Cl)$. In Kohn, M., J.F. Rakovan & J.M. Hughes, Eds., Phosphates: Geochemical, Geobiological and Materials Importance, **48, p.** 1-12. Reviews in Mineralogy and Geochemistry, Mineralogical Society of America, Chantilly, Virginia.

Hughes, J.M., and Rakovan, J. (2015) Structurally robust, chemically diverse: Apatite and apatite supergroup minerals. Elements, 11, 167-172.

Hughes, J.M., Cameron, M., and Crowley, K.D. (1989) Structural variations in natural F, OH and Cl apatites. American Mineralogist, 74, 870-876.

Hughes, J.M., Cameron, M., and Crowley, K.D. (1990) Crystal structures of natural ternary apatites: solid solution in the $Ca_5(PO_4)_3X$ (X = F, OH, Cl) system. American Mineralogist, 75, 295-304.

Hughes, J.M., Nekvasil, H., Ustunisik, G., Lindsley, D.H., Coraor, A.E., Vaughn, J., Phillips, B., McCubbin, F.M., and Woerner, W.R. (2014a) Solid solution in the fluorapatite - chlorapatite binary system: High-precision crystal structure refinements of synthetic F-Cl apatite. American Mineralogist, 99, 369-376.

Hughes, J.M., Heffernan, K.M., Goldoff, B., and Nekvasil, H. (2014b) Fluor-chlorapatite, devoid of OH, from the Three Peaks Area, Utah: The first reported structure of natural fluor-chlorapatite. Canadian Mineralogist, 52, 643-652.

Hughes, J.M., Harlov, D.H., Kelly, S.R., Rakovan J., Wilke, M. (2016) Solid solution in the apatite OH-Cl binary system: compositional dependence of solid solution mechanisms in calcium phosphate apatites along the Cl-OH binary. American Mineralogist, 101, 1783-1791.

Jenkins, H.D.B., and Thakur, K.P. (1979) Reappraisal of thermochemical radii for complex anions. Journal of Chemical Education, 56, 576-577.

Mackie, P.E., and Young, R.A. (1974) Fluorine-chlorine interaction in fluor-chlorapatite. Journal of Solid State Chemistry, 11, 319-329.

McCubbin, F.M. and Jones, R.H. (2015) Extraterrestrial Apatite: Planetary Geochemistry to Astrobiology. Elements. 11, 183-188.

McCubbin, F.M., Steele, A., Hauri, E.H., Nekvasil, H., Yamashita, S., and Hemley, R.J. (2010) Nominally hydrous magmatism on the Moon. Proceedings of the National Academy of Science, 107, No 25, 11223-11228.

McCubbin, F.M., Vander Kaaden, K.E., Tartese, R., Boyce, J.W., Mikhail, S., Whitson, E.S., Bell, A.S., Anand, M., Franchi, I.A., Wang, J.H. and Hauri, E.H. (2015) Experimental investigation of F, Cl, and OH partitioning between apatite and Fe-rich basaltic melt at 1.0-1.2 GPa and 950-1000 oC. American Mineralogist 100, 1790-1802.

Pasteris J.D., Yoder, C.H., and Wopenka, B. (2014) Molecular water in nominally unhydrated carbonated hydroxylapatite: The key to a better understanding of bone mineral. American Mineralogist, 99, 16–27.

Piccoli, P.M., and Candela, P.A. (2002) Apatite in Igneous Systems. In Kohn, M., J.F. Rakovan & J.M. Hughes, Eds., Phosphates: Geochemical, Geobiological and Materials Importance, **48, p.** 255-292. Reviews in Mineralogy and Geochemistry, Mineralogical Society of America, Chantilly, Virginia.

Rakovan, J., and Pasteris J.D. (2015) A Technological Gem: Materials, Medical, and Environmental Mineralogy of Apatite. Elements, 11, 195-200.

Sheldrick, G.M. (2008) A short history of SHELX. Acta Crystallographica, A64, 112–122.

Stock, M.J., Humphreys, M.C.S., Smith, V. C., Johnson, R.D., Pyle, D.M., and EIMF (2015) New constraints on electron beam induced halogen migration in apatite. American Mineralogist, 100, 281-293.

Stormer, J.C., and Carmichael, I.S.E. (1971) Fluorine-hydroxyl exchange in apatite and biotite: A potential igneous geothermometer. Contributions to Mineralogy and Petrology, 3l, l2l-131.

Stormer, J.C., Pierson, M.L., and Tacker, R.C. (1993) Variation of F and Cl X-ray intensity due to anisotropic diffusion in apatite during electron microprobe analysis. American Mineralogist, 78, 641–648.

Webster, J.D., Piccoli, P.M. (2015) Magmatic Apatite: A Powerful, Yet Deceptive, Mineral. Elements, 11, 167-172.

Yardley, B.W.D. (1985) Apatite composition and the fugacities of HF and HCI in metamorphic fluids. Mineralogical Magazine, 49, 77-79.

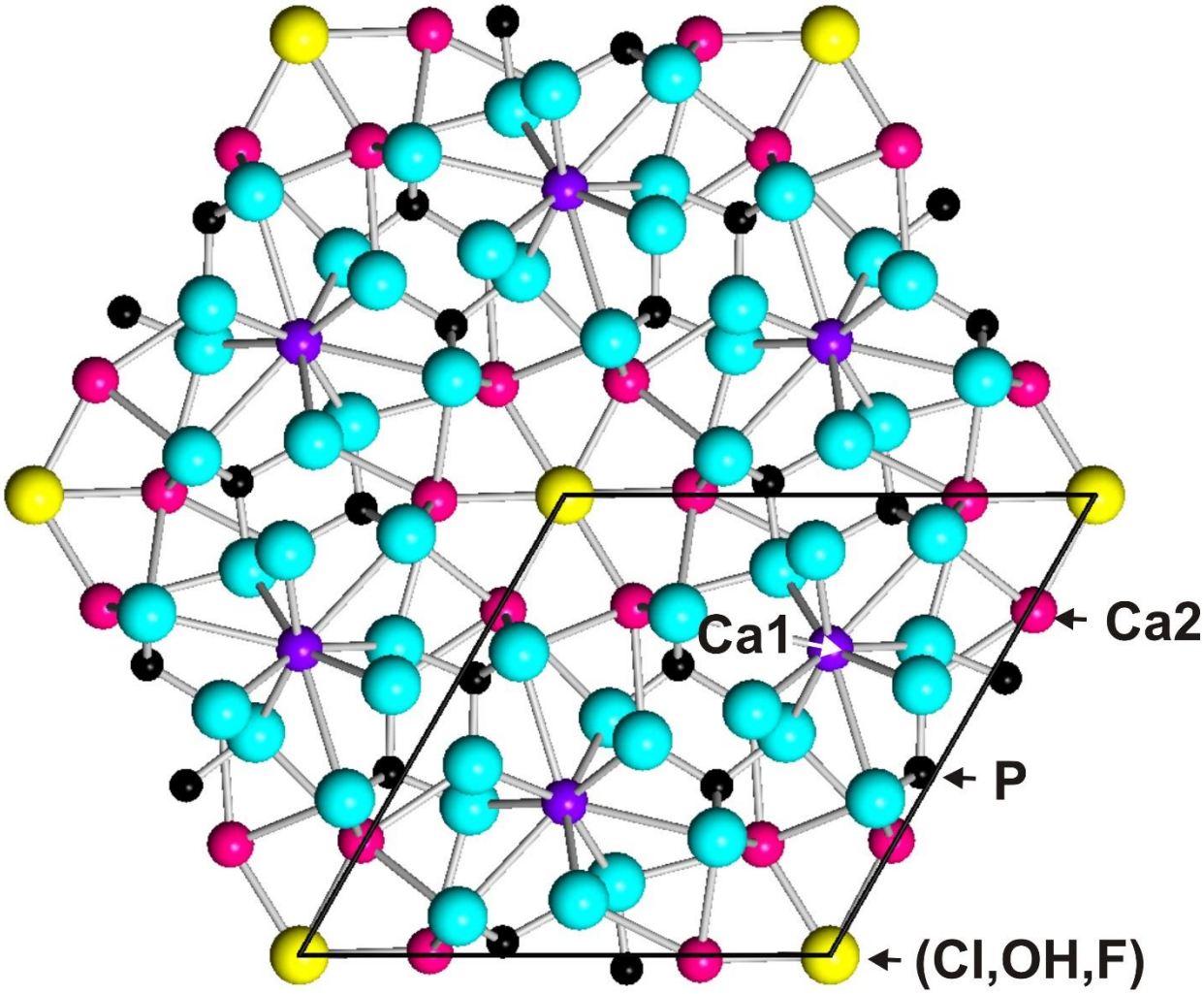

FIGURE 1. (001) projection of the crystal structure of apatite.

FIGURE 2a. A 1.2 cm tall single crystal of apatite from Kurokura, Ashigarakami district, Kanagawa Prefecture, Japan.

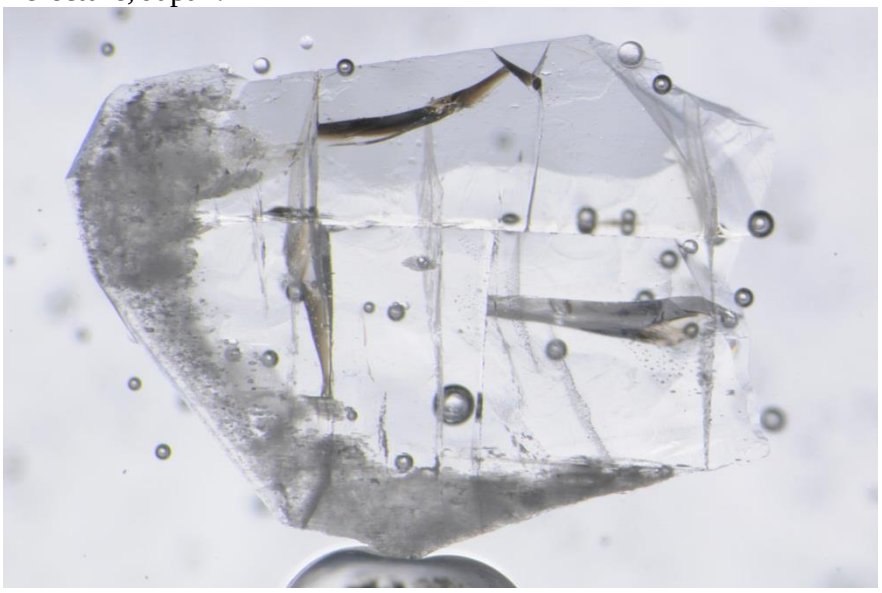

FIGURE 2b. Transmitted light image of the polished Kurokura apatite (100) section used for EMPA. Both the clear core portion of the crystal and the white, cloudy rim of the crystal are seen. The field of view in this image is approximately 5mm across. The larger bubbles seen throughout the image are air bubbles trapped in the epoxy. The sample is approximately 2 mm thick.

FIGURE 2c. Approximately 1 cm tall Kurokura apatite crystals demonstrating the white rim and clear, colorless core.

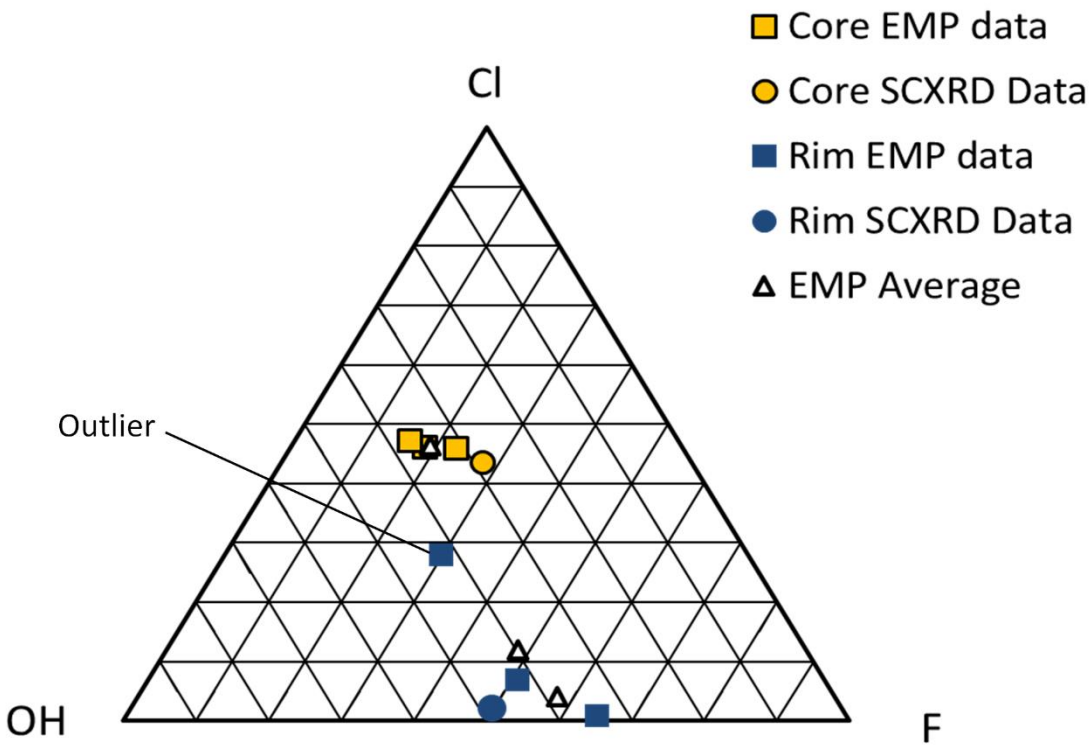

FIGURE 3. Ternary plot of the column anion chemistry (percent of total column occupancy) of the apatite rim and core from both structure refinement (SCXRD data) and electron microprobe analysis. Two averages for the rim EMPA column anion chemistry are shown, one including the outlying data point and one without.

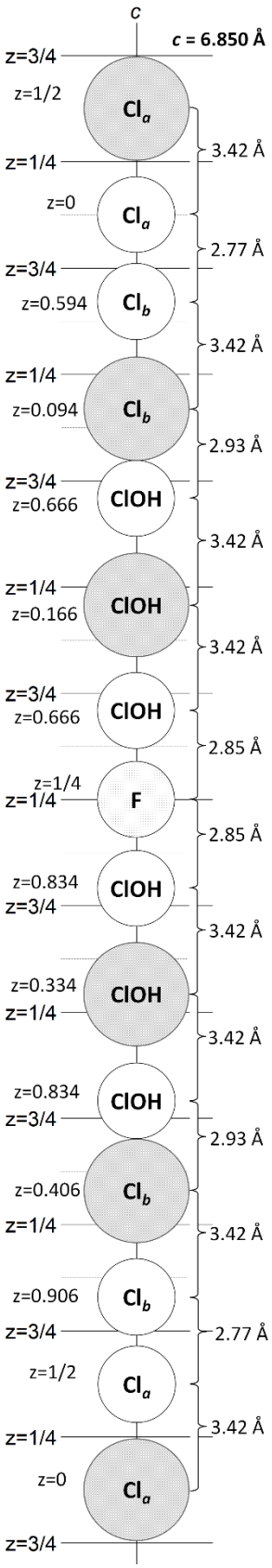

FIGURE 4. Sequence of atoms demonstrating a permissible reversal sequence of sites from above to below the mirror plane at z = 1/4 and z = 3/4 to maintain $P6_3/m$ symmetry in the Kurokura core apatite structure.

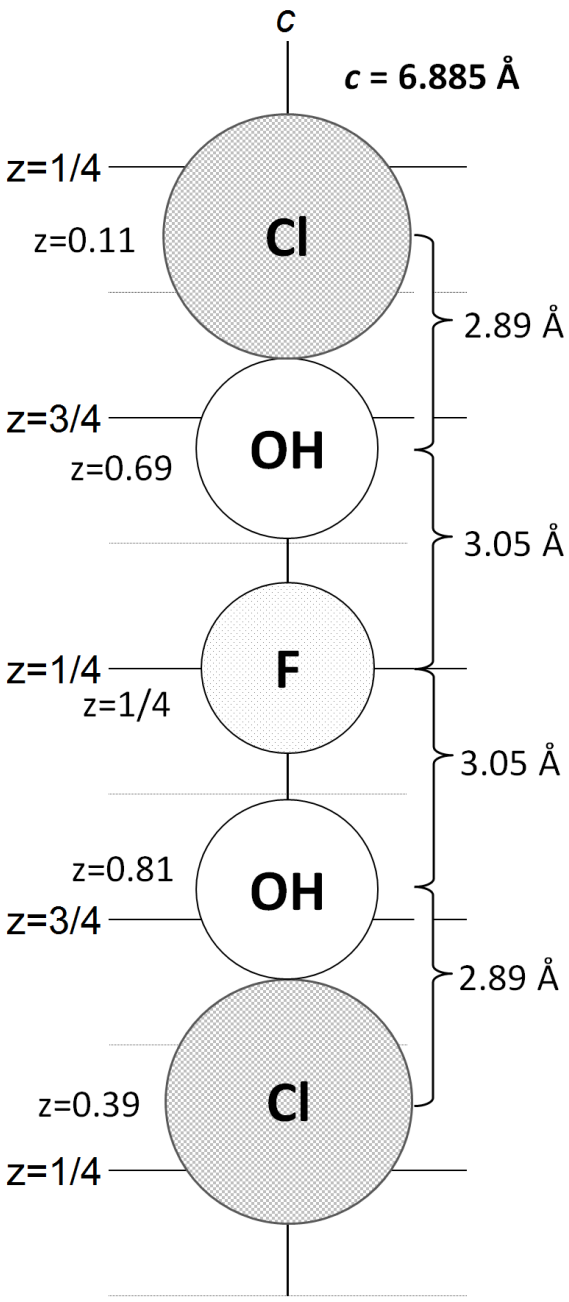

FIGURE 5. Sequence of atoms demonstrating a permissible reversal sequence of sites from above to below the mirror plane at z = 1/4 and z = 3/4 to maintain $P6_3/m$ symmetry in the Kurokura rim apatite structure.

TABLE 1. Electron microprobe chemical analysis of the Kurokura apatite. Each is an average of the three spots measured in the core and rim.

Oxide (wt.%)	Kurokura Core (n=3)			Kurokura Rim (n=3)		
CaO	53.404	±	0.328	54.998	±	0.363
F	0.716	±	0.134	1.843	±	0.689
Cl	3.244	±	0.055	0.848	±	1.005
P_2O_5	40.5	±	0.122	40.886	±	0.672
FeO	0.119	±	0.037	0.03	±	0.045
S	0.045	±	0.018	0.01	±	0.009
Nd_2O_3	0.291	±	0.048	0.136	±	0.042
Na_2O	0.168	±	0.03	0.036	±	0.052
SrO	0.024	±	0.003	0.018	±	0.005
Ce_2O_3	0.36	±	0.054	0.113	±	0.022
MnO	0.229	±	0.003	0.092	±	0.094
SiO_2	0.279	±	0.043	0.196	±	0.054
Dy_2O_3	0.051	±	0.031	0.042	±	0.024
Eu_2O_3	0.013	±	0.008	0.004	±	0.004
HO*	0.557	±	0.1	0.75	±	0.598
Total	100			100.002		
Apatite Structural Formula**						
Ca	9.659			9.792		
Na	0.055			0.012		
Fe	0.017			0.004		
Mn	0.033			0.013		
Sr	0.003			0.002		
Dy	0.003			0.002		
Eu	0.001			0.000		
Ce	0.022			0.007		
Nd	0.018			0.008		
Subtotal	9.810			9.840		
P	5.788			5.753		
Si	0.047			0.032		
S	0.014			0.003		
Subtotal	5.849			5.788		
Cl	0.928			0.240		
F	0.382			0.966		
OH*	0.664			0.875		
Subtotal	1.975			2.082		

*HO weight % and proportion in structural formula is calculated by difference.

**Apatite structural formula was calculated using atomic % values. Using net negative charge is problematic given OH substitution for F and Cl.

TABLE 2. Atomic coordinates and equivalent isotropic atomic displacement parameters (Å2) for the Kurokura core sample.

Atom	x/a	y/b	z/c	U(eq)*
Ca1	2/3	1/3	0.99794(5)	0.01099(10)
Ca2	0.2417(4)	0.9969(3)	1/4	0.0076(3)
Ca2'	0.2676(4)	0.9946(5)	1/4	0.0076(3)
P	0.62949(4)	0.03123(4)	1/4	0.00684(9)
O1	0.51310(13)	0.84692(12)	1/4	0.01300(19)
O2	0.53517(14)	0.12404(13)	1/4	0.0165(2)
O3	0.73872(10)	0.08624(10)	0.06902(13)	0.02106(19)
F	0	0	1/4	0.0130(19)
ClB	0	0	0.0942(9)	0.0106(12)
ClOH	0	0	0.1662(10)	0.0159(12)
ClA	0	0	0	0.028(10)

*U(eq) is defined as one third of the trace of the orthogonalized U_{ij} tensor.

TABLE 3. Atomic coordinates and equivalent isotropic atomic displacement parameters (Å2) for the Kurokura rim sample.

Atom	x/a	y/b	z/c	U(eq)*
Ca1	2/3	1/3	0.99875(5)	0.00896(8)
Ca2	0.2433(3)	0.99335(6)	1/4	0.0074(2)
Ca2'	0.275(6)	0.991(2)	1/4	0.0074(2)
P	0.63123(4)	0.02980(4)	1/4	0.00520(8)
O1	0.51536(13)	0.84289(13)	1/4	0.00972(19)
O2	0.53395(14)	0.12201(14)	1/4	0.0120(2)
O3	0.74258(10)	0.08495(10)	0.07029(12)	0.01393(16)
F	0	0	1/4	0.0097(14)
OH	0	0	0.193(3)	0.008(2)
Cl	0	0	0.113(13)	0.010(15)

*U(eq) is defined as one third of the trace of the orthogonalized U_{ij} tensor.

TABLE 4. Values of *z* for column anions in (0, 0, z) sites and percentage of total column anion occupancy of each corresponding site for the core structural analysis of apatite from Kurokura.

Sample	F	% Sites	Cla	% Sites	Clb	% Sites	ClOH[1]	% Sites	Column Occupancy[2]
Kurokura Core	1/4	27.7	0	3.0	0.094	25.4	0.166	44.00	$F_{0.55}(OH)_{0.58}Cl_{0.87}$

[1]ClOH site: 65% OH, 35% Cl

[2]Constrained to 2.00 column anions/formula unit

TABLE 5. Values of *z* for column anions in (0, 0, z) sites and percentage of total column anion occupancy of each corresponding site for the rim structural analysis of apatite from Kurokura.

Sample	F	% Sites	Clb	% Sites	OH	% Sites	Column occupancy
Kurokura Rim	1/4	52.6	0.113	2.1	0.193	51.0	$F_{1.05}(OH)_{1.02}Cl_{0.04}$